International Journal of Scientific & Engineering Research
ISSN 2229-5518

GOVERNMENT COLLEGE UNIVERSITY FAISALABAD, PAKISTAN

MODULATION OF ZnO PROPERTIES

Khalid Mahmood

IJSER

DEPARTMENT OF PHYSICS

Abstract

One of the mysteries of ZnO materials is defect chemistry and its role in tailoring the material properties. Besides of its wide band gap and large exciton binding energy, ZnO has plenty of intrinsic defects which can strongly influenced the structural, optical, electrical and thermoelectric properties related with this material. Therefore the identification, control and effects of intrinsic defects on ZnO material properties is always very important topic of study among the researchers engaged in ZnO based research.

The modulation, control of intrinsic defects and their role in tailoring the structural, optical, electrical and thermoelectric of ZnO has been investigated comprehensively in this thesis. Three methods have been employed to vary the density of intrinsic defects; By changing the growth conditions of MBE reactor (Zn/O contents ratio from 1.08 to 1.22), annealing in different environments (oxygen, zinc, vacuum and successively annealed in vacuum and zinc), annealing in oxygen at different temperature (500 ^{0}C to 1000 ^{0}C) and using high pressure (MPa) high temperature condition of MBE grown samples on Si (100) substrate.

XRD, FTIR and PL measurements were performed on these three types of samples to investigate the structural and optical properties. All samples showing strong ZnO (002) plane suggested the c-axis growth of samples. The FWHM of this peak increased with increasing Zn/O contents ratio, while annealing in vacuum, zinc, successively annealed in vacuum-zinc and decreased as the annealing temperature increased from 500 ^{0}C to 800 ^{0}C. The PL measurements also confirmed the XRD results that crystal quality degrades as the Zn/O contents ratio increased. The detailed investigation on the origin of defect emission from was performed by annealing samples

IJSER

in different annealing environments and related it with transition involving zinc interstitial and oxygen interstitial.

Hall measurements suggested that carrier concentration increased with higher Zn/O ratio, annealing in vacuum, zinc and successively annealed in vacuum and zinc but decreased while annealed in oxygen environment at different temperature. A defect donor complex V_O-Zn_i was identified as source of intrinsic n-type conductivity of ZnO.

In order to study the electrical properties, Au metal contacts were fabricated on all sample using similar evaporation conditions. DLTS study was suggested that all samples have similar kind of donor deep level defects having activation energy 0.53 eV below the conduction band. Therefore another sample with high oxygen ratio was chosen for further DLTS measurements. This sample consists of a deep acceptor level and after detail investigation; we related it with Zn-vacancy related complex. This defect also showed meta-stable behavior with time.

IJSER

Chapter 1 Introduction and Motivation

1.1 Introduction

Thanks to its wide band gap (3.37 eV) and high exciton binding energy (60 meV) at room temperature [1], ZnO is a material of today's research. The wide bang gap of ZnO makes it an ideal candidate for electronic and optoelectronic devices operating at short wavelengths. The examples of these devices includes ultra violet light emitting diodes (UV-LED), UV detectors, Bacteria killer devices, surface acoustic wave devices, sensors, flat panel displays, transparent thin films transistors and transparent conducting electrodes for solar cells [2-6]. The large exciton binding energy leads to lasing action based on exciton recombination and polariton/exciton interaction even at room temperature.

The new and emerging field of Spintronic is highly based on the transition metals doped ZnO material. High temperature ferromagnetism has been observed from transition metals doped ZnO such as Mn, Co and Fe for practical Curie temperatures [7].

IJSER

When we compare ZnO with other wide band gap semiconductors like GaN, it has some superior properties over GaN like high luminescence efficiency of light emission due to larger exciton binding energy of about 35 meV higher than GaN [8]. ZnO has exhibited better radiation resistance than GaN for possible devices used in space and nuclear applications. ZnO can be grown in bulk and on cheaper substrates like glass. The presence of ZnO native substrate is highly appreciated because the defect density would be remarkably decreased in homo-epitaxy. Unfortunately GaN is lacking in homo-epitaxy, therefore has high density of extended defects.

Band gap tailoring is another important aspect of ZnO. The band gap of ZnO can be engineered from 7.8 eV to about 2.3 eV by adding Mg and Cd. The addition of Mg increases the band gap of ZnO and Cd decreases the band gap [9].

The sensing property of ZnO to sense many gases is its forefront advantage to use this material in sensors and actuators [10]. Therefore ZnO can be used as a sensor to smell the freshness of food and drinks. Furthermore ZnO has large piezoelectric constant (applied deformation in the crystal generates voltage and vice versa). This property is basic building block of sensors, transducers and actuators.

ZnO has rich intrinsic defect chemistry, which highly influenced the above mention properties of ZnO. It is believed that the intentionally n-type conductivity of ZnO is due to intrinsic defects present in the band gap [11]. The structural, optical, electrical and thermoelectric properties can be modified with the presence of intrinsic defects in ZnO.

IJSER

In addition, ZnO can be grown in many nanostructures like nano-rods, nanowires, nanobelts, nano-combs, nano-generators and nanotubes [12-15]. As nanostructures strongly enhanced the magnetic field, therefore they can be used as field emitters and nano-sized read/write heads of data storage devices.

1.2 Issues Related with ZnO

Despite the fruits offered by the ZnO, there are many issues related with ZnO material and devices to become commercial. These issues should be comprehended in order to get full advantage of amazing benefits of ZnO.

The first and changeling issue related with ZnO is p-type conductivity control. Although many reports claimed the p-type conductivity, but reproducible p-type conductivity with high hole

concentration and mobility, is still a changeling. ZnO naturally is an n-type material due to the presence of shallow native defects such as oxygen vacancies (V_O) and zinc interstitials (Zn_i) [16]. These defects compensate the acceptor doping density and prevent the p-type conductivity.

The luminescence from ZnO is also still under debate. The visible emission from ZnO is considered to be due to intrinsic defects, which form a deep level defect in the band gap of ZnO, but the responsible defect is not cleared yet, because controversial results have been published in literature [16, 17].

The ZnO is facing another issue; that is the origin of intrinsic n-type conductivity. Naturally ZnO is n-type semiconductor with high electron concentration of about 10^{20} cm^{-3}. But researchers are not arriving to a conclusion that either this electron concentration is due to oxygen vacancy or zinc interstitial.

IJSER

The reliable Ohmic and Schottky contacts, which work at high temperature and harsh environment, are also a matter of difficulty to use ZnO in practical devices.

The selection of proper growth technique for ZnO materials has key importance to grow defect free material for devices because the concentration of intrinsic defects and impurities are related to growth conditions. Several growth techniques have been found in literature for the growth of high quality ZnO such as hydrothermal, sputtering, pulsed laser deposition (PLD), chemical vapor deposition (CVD) and molecular beam epitaxy (MBE). So the selection of appropriate growth technique is highly desirable and comprehended.

Figure 1Summery of work carried out in this dissertation

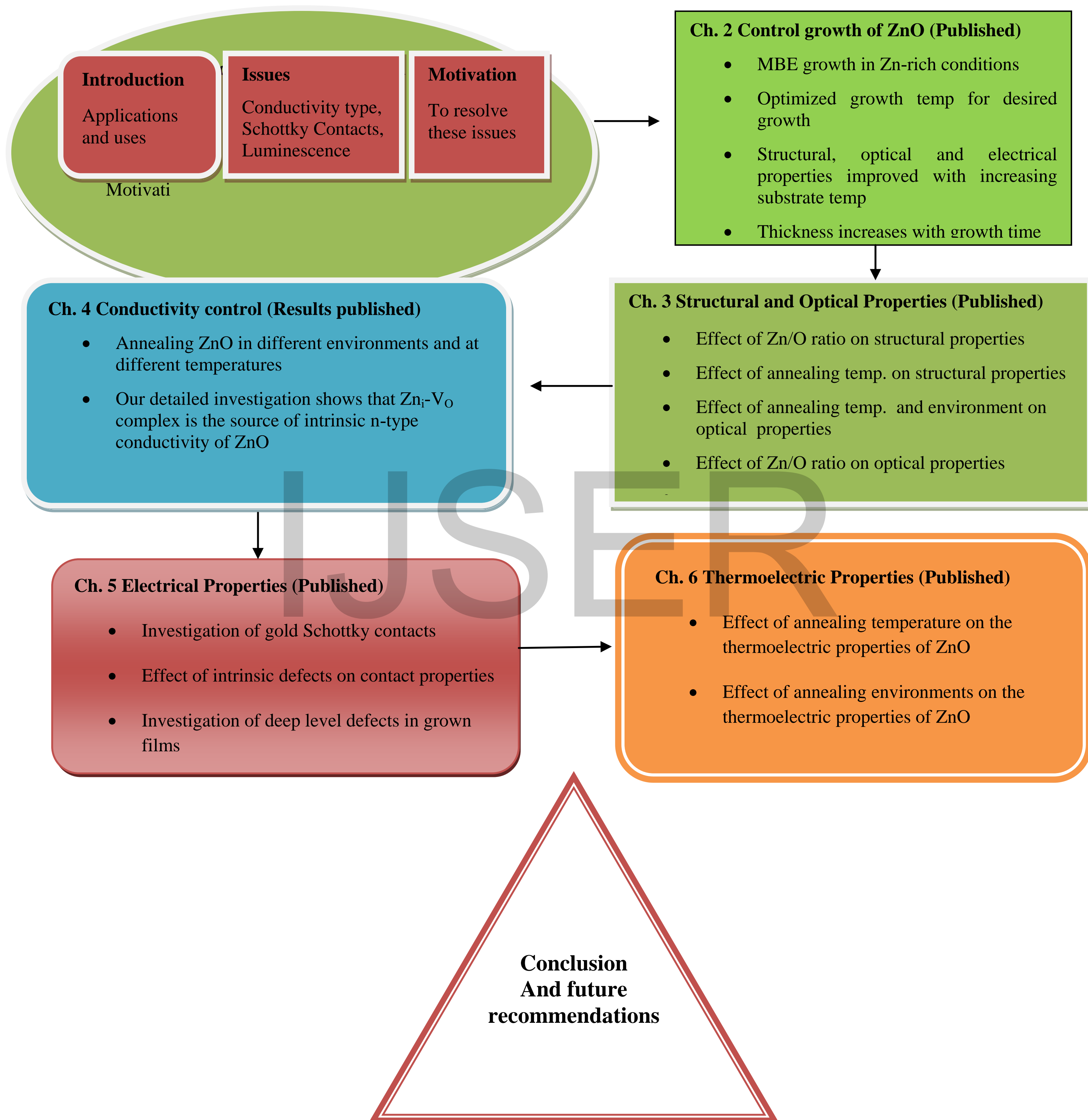

IJSER

1.3 Motivation for this work

Controlling the intrinsic defects and their properties is a basic requirement for ZnO to use it in practical devices. As the very little concentration of intrinsic defects and impurities may greatly modifies the structural, optical and electrical properties, therefore complete understanding of intrinsic defect chemistry (Zinc interstitials, Oxygen vacancies, Zinc vacancy, Oxygen interstitials, Zinc antisites, Oxygen antisites) and their affects on structural, optical, electrical and thermoelectric properties of ZnO is of fundamental interest. In this dissertation, the effect of intrinsic defects on the above mention issues related with ZnO will be highlighted in detail, to resolve these non profitable matters in order to fully utilize the benefits offered by ZnO.

We can divide this thesis into three parts

IJSER

1. Control growth of ZnO by MBE in Zn-rich conditions to obtained the higher density of defects (Zn-interstitials, Oxygen vacancies) and also optimized the growth parameters for MBE grown ZnO for desired properties.
2. The density of intrinsic defects was modulated by two ways;
   (i) By changing the growth conditions like substrate temperature and Zn-cell temperature in MBE reactor and have grown a batch of samples with different Zn/O ratio
   (ii) A representative wafer was cut into small pieces and annealed in different annealing environments such as oxygen, zinc, vacuum and successively annealed in zinc and vacuum for one hour. Another set of samples was annealed in oxygen environment for one hour at different temperatures from 500 to 800 ^{0}C.

(iii) Apply high pressure in GP to modulate the defect density in ZnO and study the effect of changing defect concentration on the structural, optical and electrical properties of ZnO. Only few experiments of such kinds have been performed using hydraulic machine at Department of Geology, University of California Los Angeles, USA. This study is still under investigation, therefore results have not been reported in this dissertation.

3. Study the influence of intrinsic defects on the structural, optical, electrical and thermoelectric properties of ZnO using different characterization techniques such X-Ray Diffraction (XRD), Photoluminescence (PL), Raman Spectroscopy, Energy Dispersive X-ray Diffraction (EDAX), Fourier Transform Infrared Spectroscopy (FTIR), Seekbeck Effect, Current-Voltage (I-V) Measurements, Capacitance-Voltage (C-V) Measurements, Deep Level Transient Spectroscopy (DLTS) and Hall Measurements.

IJSER

1.4 References

[1] M. Asghar, K. Mahmood, I. Ferguson, M-Y Raja, R. Tsu, Y-H Xie, M-A Hasan, Semi. Cond. Sci. Technol. 28 (2013) 105019

[2] Q. Humayun, M. Kashif, U. Hashim, Optik 124 (2013) 5961

[3] J-H. Lee, B. Hong, Y.S. Park, Thin Solid Films 547 (2013) 3

[4] M. Mahanti, D. Basak, J. Lumin. 145 (2014) 19

[5] D-H. Jin, D. Kim, Y. Seo, H. Park, Y-D. Huh, Mater. Lett. 115 (2014) 205

[6] S. Sarkar, D. Basak, Sens. Actuators B: Chem. 176 (2013) 374–378

[7] W. Yan , Q. Jiang , Z. Sun , T. Yao , F. Hu, S. Wei, J. Appl. Phys. 108 (2010) 013901

[8] H. Zeng, G. Duan, Y. Li, S. Yang, X. Xu, W. Cai, Adv. Funct. Mater. 20 (2010) 561

[9] Q. Shi, Z. Wang, Y. Liu, B. Yang, G. Wang, W. Wang, J. Zhang, J. Alloy. Comp. 553 (2013) 172

[10] P. Rai, R. Khan, R. Ahmad, Y-B Hahn, I-H Lee, Y-T Yu, Current Appl. Phys. 13 (2013) 1369

[11] M. Asghar, K. Mahmood, M-A Hasan, J. Key Eng. Mater. 510 (2012) 227

[12] M. Asghar, K. Mahmood, Yasin A Raja, M-A Hasan, Adv. Mater. Research 622-623 (2012) 919-924

[13] Z. L. Wang, J. Phys: Condens. Matter 16 (2004) R829

[14] S. Tian, D. Zeng, X. Peng, S. Zhang, C. Xie, Sensors and Actuators B 181 (2013) 509–517

IJSER

[15] L. Feng, A. Liu, M. Liu, Y. Ma, J. Wei, B. Man, Mater Characterization, 61 (2010) 128

[16] M.D. McCluskey, S.J. Jokela, J. Appl. Phys. 106 (2009) 071101

[17] A. Janoti, Chris G Van de Walle, Rep. Prog. Phys. 72 (2009) 126501

IJSER

Chapter 2 Experimental Work

2.1 Introduction

The selection of proper growth technique is very important for the growth of ZnO because the properties of grown samples are strongly depends upon the growth conditions and technique used. The density of intrinsic defects varies from sample to sample which has grown from two different techniques. In literature we have find a number of growth techniques including hydrothermal growth [1], pulsed laser deposition (PLD) [2], sol-gel technique [3], sputtering [4], chemical vapor deposition (CVD) [5] and molecular beam epitaxy (MBE) [6]. All techniques associated with some advantages and disadvantages. The most frequently used technique for bulk growth of ZnO is hydrothermal technique. The main advantage of this technique is large wafer growth, up to 3 inch, can be grown easily. The other advantages includes; high crystal quality, low dislocation density and alloys. Despite of its many favorable points, core problem associated with hydrothermal growth is lack of control of p-type conductivity [7].

PLD is another commonly used technique because one can find thousands of research papers on this technique. The prime advantages of PLD growth technique are; it has multi-components sources, low temperature growth technique, high quality thin films obtained and set up is very simple. The drawback of PLD is that is very difficult to control the intrinsic defect density [8].

IJSER

Figure 2 Flow chart of work done in chapter 2

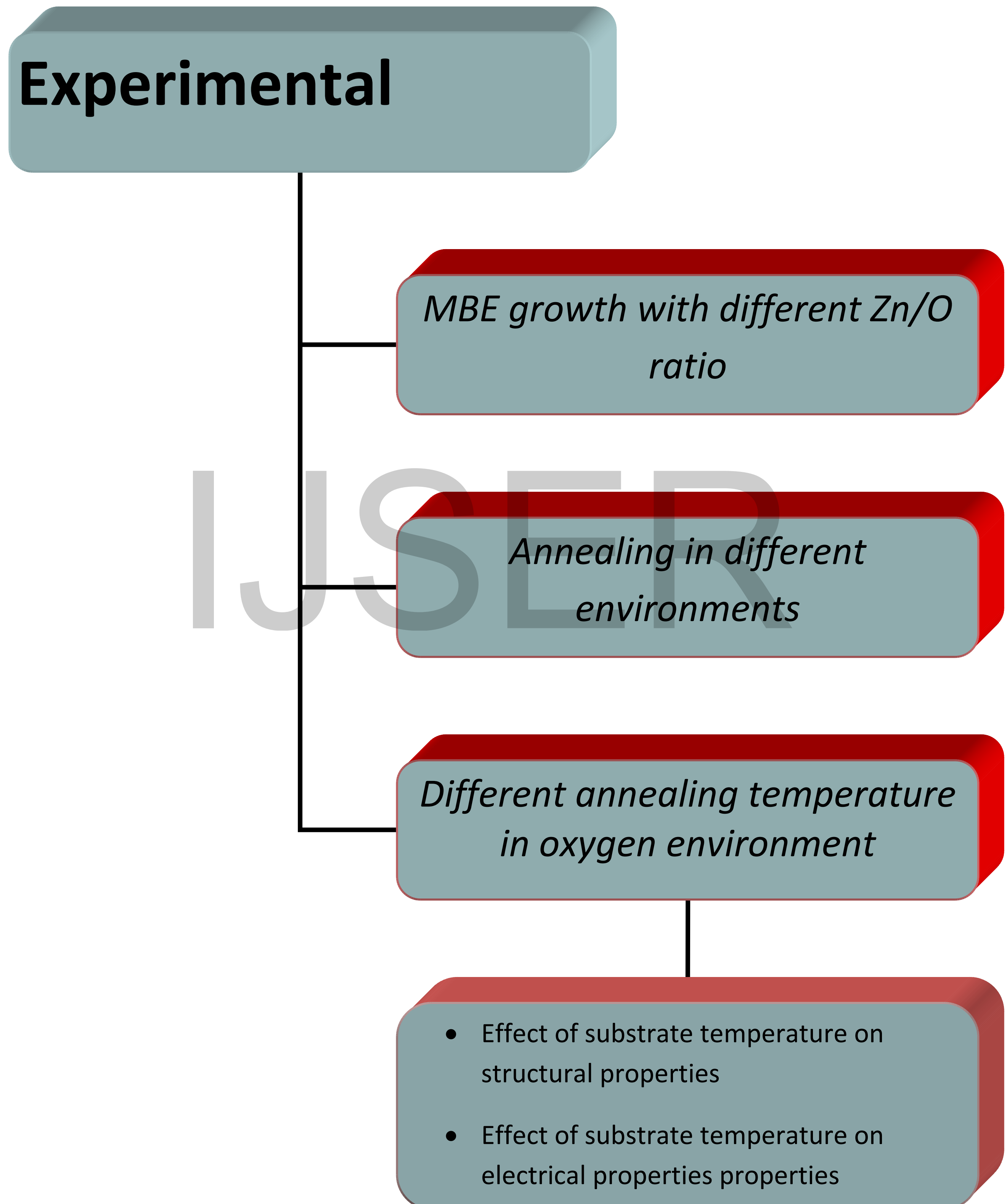

IJSER

Due to simple growth mechanism, Sputtering is also widely used growth technique. The cost of sputtering technique is very low and set is very simple. The operating temperature of sputtering is also low and the quality of grown film is also reasonable. The grown films of ZnO grown by sputtering are usually polycrystalline which is the demerit of this technique [9].

Chemical vapor deposition (CVD) is also very common technique for ZnO among the researchers community. In CVD growth method, ZnO deposition occurs as a result of chemical reactions of vapor-phase precursors on the substrate, which are delivered into growth zone by the carrier gas. The reactions take place in a reactor where a necessary temperature profile is created in the gas flow direction. High crystalline large area ZnO wafers can be grown by CVD but the control of Zn/O contents ratio is very hard to achieve [10].

IJSER

On the basses of summery of different growth techniques presented above, we come to a conclusion that all growth techniques have advantages and limitations depends upon the properties you want to achieve. But none of the above mention techniques is capable of producing high quality films with controlled density of intrinsic defects. It is also concluded that none of the technique is capable of growing ZnO with controlled Zn/O contents ratio.

2.2 Molecular Beam Epitaxy – An Overview

The first use of molecular beam epitaxy dates back to 1970, when it was used for the growth of GaAs [11]. The schematic diagram of MBE system is shown in fig. 2.1. It consists of a vacuum chamber with RF source. Roughing and high vacuum pumps are connected with chamber to achieve ultra high vacuum conditions. There is a shutter between Zn-cell and substrate to allow the Zn contents to deposit on the substrate. The pure Zn is evaporated from effusion cell and oxygen is supplied from a radio frequency source. Both Zn and Oxygen continents arrived at

heated substrate and different process occurred in sequence; adsorption, desorption, self diffusion, incorporation and decomposition. The growth rate is normally 1 μm/h or slightly more than one monolayer per second [12].

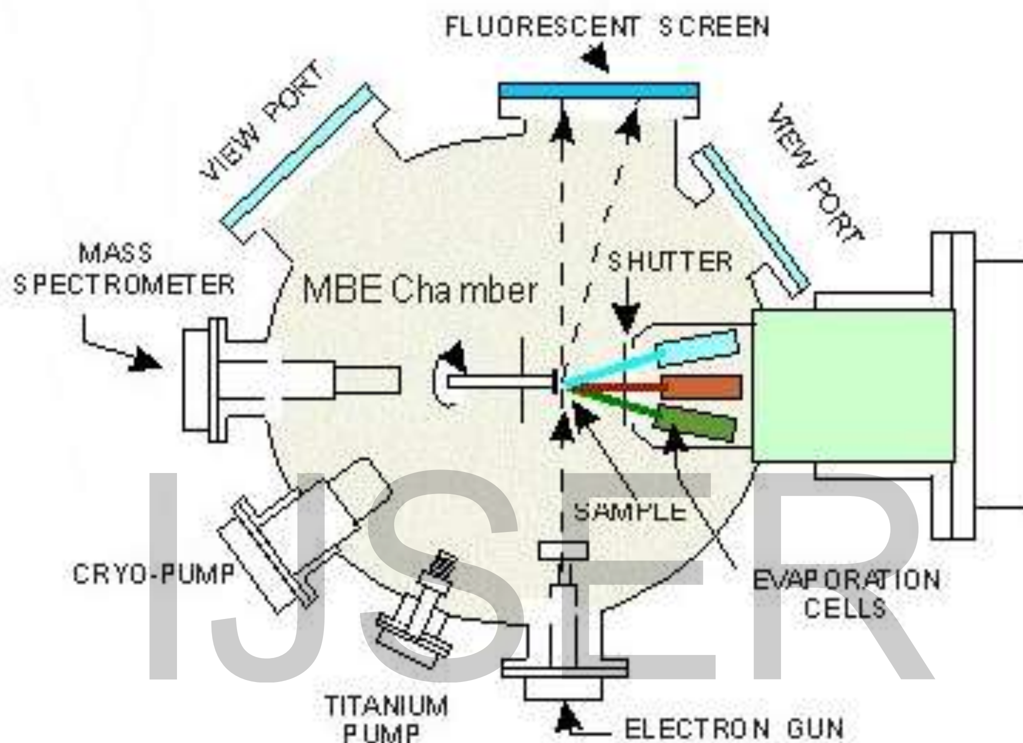

Figure 3 Schematic diagram of MBE system

MBE is extremely important and versatile technique in the sense that one can grow both elemental and compound semiconductor with high purity. Furthermore MBE is ultra vacuum technique therefore many surface diagnostic instruments attached with MBE chamber, such as photoemission spectroscopy, field emission spectroscopy, molecular beam and ion beam scattering spectroscopy and Raman scattering spectroscopy, for the insitu measurements of surface properties of materials. Molecular beam epitaxy can be used to achieve extreme dimensional control in both chemical composition and doping profile. Single crystal multilayered structures with dimension of only few atomic layers can be grown. MBE is also used for the

growth of abrupt interfaces and doping variation devices with desirable transport properties and optical properties [13].

2.3 Growth Conditions

The substrate temperature and Zn cell temperature are very important parameters for the control growth of ZnO by MBE. By varying these two parameters, one can control the deposition rate of films and also modulate the ratio of Zn/O. Therefore MBE growth technique is used in this study to precisely control the Zn/O ratio. Furthermore the density of intrinsic defects is directly related with Zn/O ratio; therefore by controlling the Zn/O ratio we have modulated the density of intrinsic defects in ZnO.

In this study about thirty samples were grown with different growth conditions to modulate the density of intrinsic defects. The growth conditions within 0.5% tolerance for A, B, C and D samples were set as following: substrate temperature: $200^{o}C$, $300^{o}C$, $400^{o}C$ and $500^{o}C$ respectively, temperature of the Zn-Knudsen cell: $296^{o}C$, Zn beads purity 99.9999%, pressure of the chamber during the growth was ~ 1×10^{-4} mbar (2×10^{-4} mbar) and oxygen plasma was generated by RF power supply operated at 300W.

IJSER

2.4 Annealing Experiment

The density of intrinsic defects was also modulated by annealing experiments. A representative sample was cut into 1cmx1cm pieces and subject to different annealing treatments. For annealing purposes two types of furnaces were used; tube furnace and vacuum furnace. Oxygen annealing was done using the flow of pure oxygen gas with flow rate of 50 sccm. To suppress the effects of impurities, flow of nitrogen was also introduced into the furnace. For annealing in vacuum environment, we have used vacuum furnace having chamber pressure 4×10^{-7} torr. This pressure

was attained by using rotary and diffusion pumps. When the pressure was attained, heating element was operated to gain the annealing temperature.

2.4.1 Step 1

In first step of annealing process, samples were annealed in oxygen environment at different temperature from 500 to 800 ^{o}C, keeping a step of 100 ^{o}C for one hour (Detail can be shown in table 1.)

Table 1 Detail of annealing temperature of MBE grown ZnO on Si substrate

Annealing Environment	Annealing Temp. (^{o}C)	Annealing Time (Mints)
Un-annealed	-	-
Oxygen	500	60
Oxygen	600	60
Oxygen	700	60
Oxygen	800	60

IJSER

4.2.2 Step 2

In second step of annealing experiment, grown samples were annealed in different environments such as oxygen, vacuum, zinc and successively annealed in vacuum and zinc at 600 ^{o}C for one hour shown in table 2. Annealing in zinc environment was performed by placing zinc powder on sample surface and heated. The zinc vapors diffuse into the sample at high annealing temperature.

Table 2 Detail of MBE grown samples annealed in different environments

Annealing Environment	Annealing Temp. (^{o}C)	Annealing Time (Mints)
Un-annealed	-	-
Zn-vapor	600	60
O_2	600	60
Vacuum	600	60
Zn in Vacuum	600	60

2.5 Measurements Techniques

2.5.1 X-Ray Diffraction (XRD)

X-Ray Diffraction (XRD) was performed to investigate the crystal structure, lattice constant, stress in films, crystal orientation and crystalline size of grown samples. The XRD is versatile technique in a sense that it can measure any sample but the sensitivity depends upon the material used [15]. XRD measurements were performed using Panlatical x-ray diffrecto-meter having Cu_{α} source with wavelength 1.54 A^0. The XRD facility was used at University of North Carolina Charlotte, USA.

2.5.2 Photoluminescence (PL)/Raman Spectroscopy

Photoluminescence is a very strong technique to detect and identify impurities in the band gap of semiconductor materials. PL relies on the creation of electron-hole pairs by incident radiation and subsequent radiative photon emission. The intensity of emitted photon is directly related with the density of impurities [16]. The set up of PL consists of three major parts; Laser, monochromat and detector. For PL measurements, we have used mini PL/Raman system having

IJSER

Cd-Ne laser with photon wavelength 248 nm. Impurity identification by PL is very precise because the energy resolution is very high. It is the density measurement that is more difficult because it is not easy to draw a correlation between the intensity of a given impurity spectral line and the density of that impurity.

2.5.3 Hall Effect

The Hall effect, which was discovered in 1879 (Hall, 1879), determines the concentration and type (negative or positive) of charge carriers, mobility and resistivity in metals and semiconductors. The key parameter in determining the carrier density is Hall coefficient which can be determined using following equation [17].

$$R_H = tV_H/BI$$

Where t is sample thickness, V is applied voltage, I is current and B is magnetic field. The carrier concentration is related with Hall coefficient by relation

$$R_H = -1/ne$$

Where e is electronic charge and n is carrier concentration.

Ecopia 3000 Hall system having magnetic field 0.5 T, was used in this study to measure doping concentration, mobility and resistivity of all samples. All the measurements were performed at room temperature.

2.5.4 Deep Level Transient Spectroscopy (DLTS)

DLTS is a widely adopted method for detection and characterization of deep levels contained in materials and devices. It was developed in 1974 by Lang [18] and implemented by Miller [19] and Kimerling [20]. The fundamental point is the measurement of transients of differential capacitance of the space charge region under electrical pulses of p–n junctions, Schottky diodes or MIS (metal–insulator semiconductor) structures.

IJSER

By measuring capacitance or current transients which can be produced when we pulsing the semiconductor junction at different temperatures, a spectrum is produced which show a peak for each deep levels. This method has provided a good tool for the understanding of materials processing for semiconductor devices. The DLS-83 Hungry was used for the measurements of I-V characteristics, C-V characteristics and identification of deep level defects in band gap.

2.6 Effect of Substrate temperature on structural properties

Substrate temperature is very important parameter for controlling the Zn/O contents ratio. The variation of substrate temperature during growth affects the deposition rate and also the crystallinity of films due to excess Zinc or Oxygen vacancy [21]. The resistivity and mobility of films are also related to the substrate temperature.

IJSER

Fig.4 demonstrated the typical XRD pattern of the as grown samples A, B, C and D. Two distinct peaks were observed at angles (2θ) 34.47^0 and 72.4^0 from all samples representing the (002) and (004) planes of ZnO, respectively [22]. Peak (002) being the dominant among the others, indicates that the preferable direction of the growth is along this plane i.e. *c*-plane. No typical diffraction peak from Zinc or other impurities have been found in any of our samples.

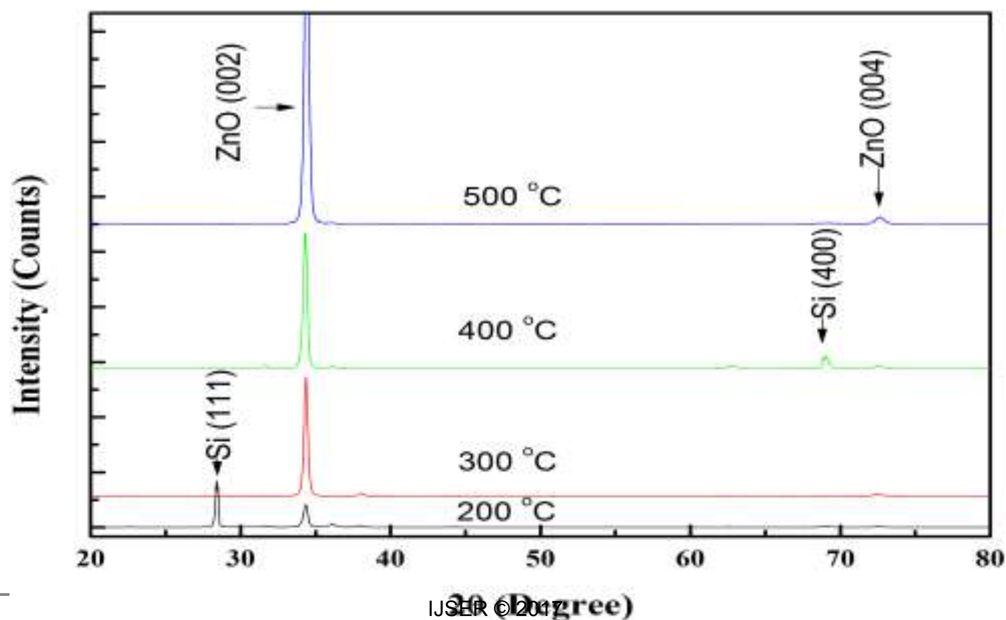

Figure 4 Typical XRD patterns of MBE grown samples with different substrate temperatures. The graph shows that growth direction is along c-axis

We have observed that the position of ZnO (002) peak remains constant, but its intensity increases as the substrate temperature increases from 200 ^{0}C to 500 ^{0}C. The possible reason is that at low substrate temperature stress exists within the layers and it progressively decreased with increasing substrate temperature in our measurement regime. Furthermore as the substrate temperature decreases, atoms have not sufficient mobility to fill the appropriate lattice sites which results in the degradation of crystal structure [23].

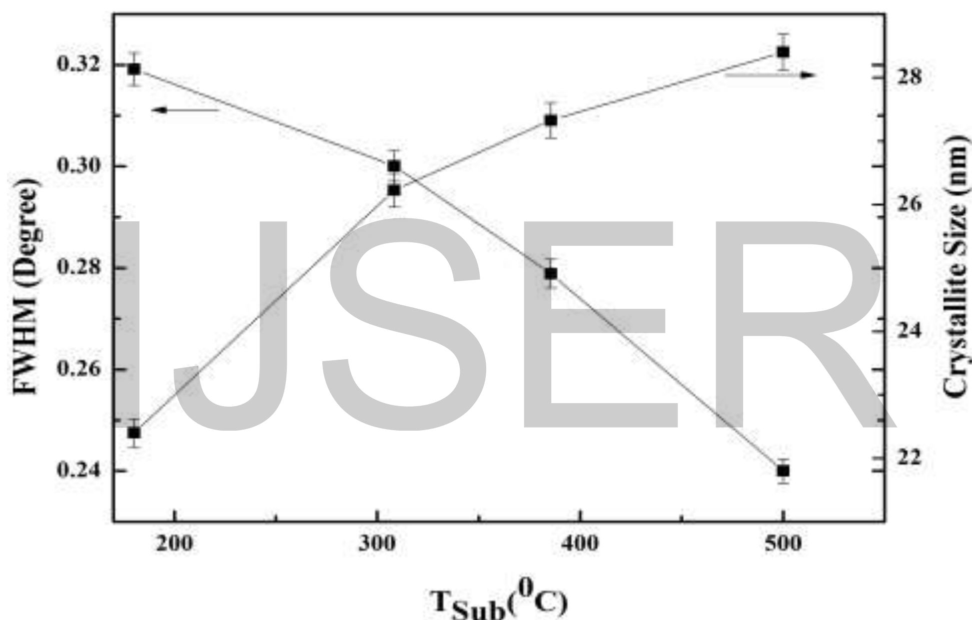

Figure 5 The relationship of substrate temperature with FWHM and crystallite size. The crystal quality of films improved with increasing substrate temperature

Fig. 5 shows the effect of substrate temperature on the full width half maximum (FWHM) and crystallite size of grown films. The crystalline size of samples were calculated by using Scherer's formula in Eq. below

$$P = \frac{\lambda}{\beta Cos\theta}$$

where λ is wavelength of Cu, k_{α} radiations (1.54 A^{0}), β is FWHM of ZnO (002) peak.

The figure shows that FWHM of ZnO (002) peak is decreased from 0.32^0 to 0.25^0 and crystallite size increased from 23 nm to 29 nm as the substrate temperature increased from 200 to 500 ^{0}C. The smaller value of FWHM represents the good crystanality of grown films. The lowest value of FWHM and maximum value of crystallite size is observe at substrate temperature 500 ^{0}C.

2.7 Effect of substrate temperature on electrical properties

Fig. 6 shows the relationship of substrate temperature and thickness of films. The film thickness increases from 0.3 µm to 1.5 µm as substrate increases from 70 ^{0}C to 500 ^{0}C (detail can be shown in table 3). The high substrate temperature facilitates the atoms arriving on the surface of substrate to move quickly to look for the lowest energy sites and form the low energy structure. Consequently the micro-structure of films grown at high substrate temperatures improves significantly.

IJSER

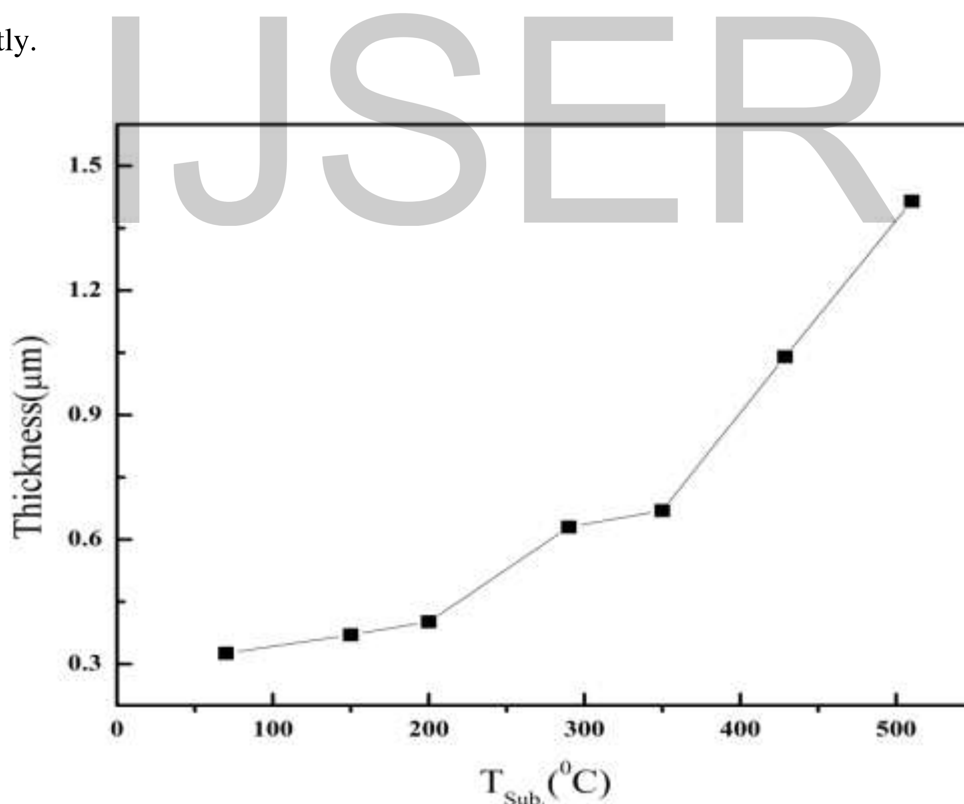

Figure 6 Plot between substrate temperature and thickness of grown films

As a result, the thickness of the ZnO thin film deposited at high substrate temperature is larger than the sample deposited at lower substrate temperature.

Fig. 7 shows the dependence of carrier concentration and resistivity of ZnO layers on the substrate temperature. The carrier concentration decreased from $2.2\times10^{19}\pm1$ cm^{-3} to $5.0\times10^{16}\pm1$ $cm^{-3}$and resistivity increased from 1.1±0.01 Ω cm to1.7±0.01 Ω cm for samples with increasing substrate temperature from 200 ^{0}C to 500 ^{0}C respectively.

Table 3 Effect of substrate temperature on FWHM, crystalline size, carrier concentration, resistivity and thickness of MBE gown samples

Sr. No	$T_{sub.}$ (^{0}C)	FWHM (Degree)	Crystalline Size (nm)	Carrier Concentration (cm^{-3})	Resistivity (Ω cm)	Thickness (μm)
1	200	0.32	23	$2.2x10^{19}$	1.1	0.4
2	300	0.30	26	$1x10^{18}$	1.62	0.6
3	400	0.28	27	$1.1x10^{17}$	1.35	0.95
4	500	0.25	29	$5x10^{16}$	1.7	1.6

IJSER

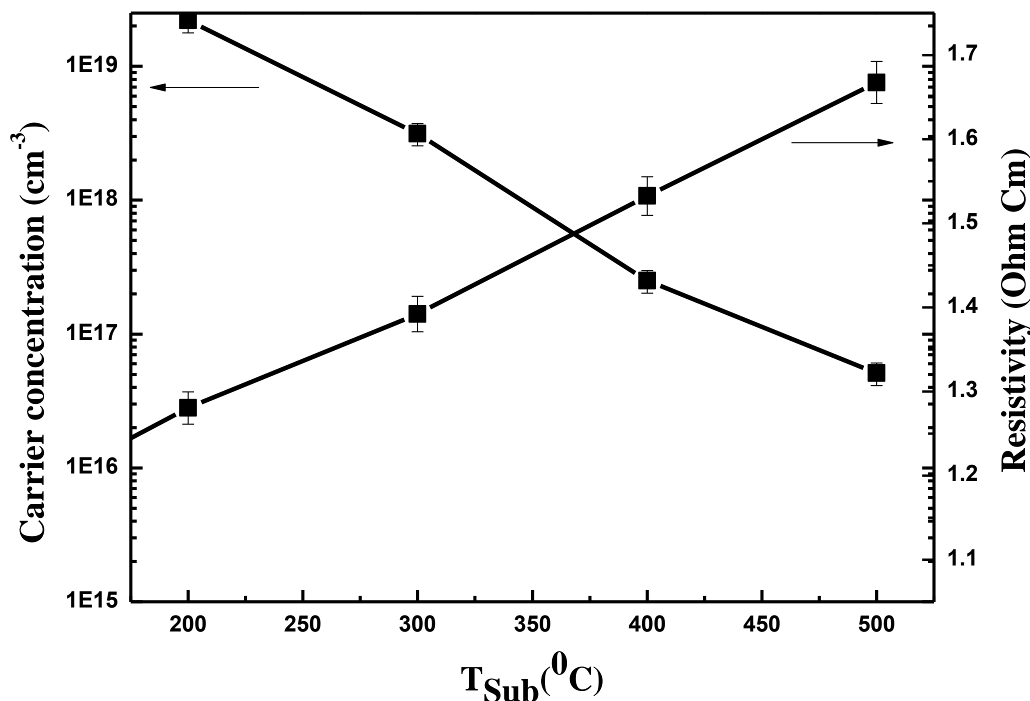

Figure 7 The dependence of carrier concentration and resistivity of measured samples on the substrate temperature

We argue that the observed n-type conductivity of samples is due to intrinsic donors defects like Zn-interstitials, Oxygen vacancies or complex of both. The density of intrinsic donor defects decreased with increasing substrate temperature as evident by XRD measurements. As the carrier concentration is attributed to V_O-Zn_i complex (explained in Ch.4), therefore the density of these defects decreased at higher substrate temperature which owing to the reduction of carrier concentration.

IJSER

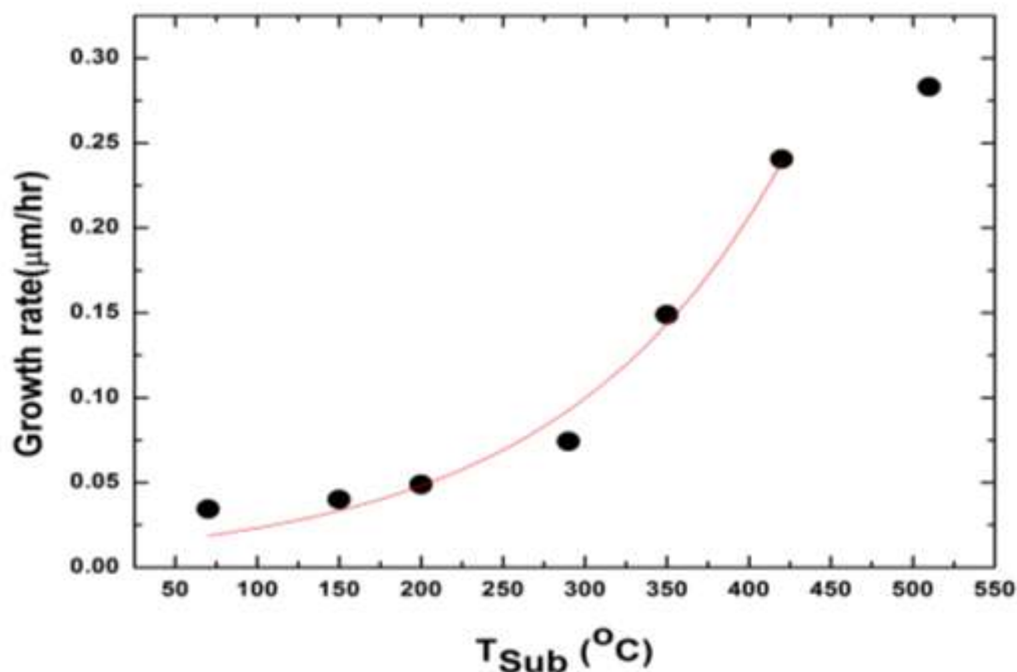

Figure 8 Effect of substrate temperature on the growth rate of ZnO thin films

Fig 8 shows the relationship between substrate temperature and growth rate of film. The graph revealed that growth rate has linear relationship with substrate temperature. The possible reason of this effect is that at high substrate temperature the diffusivity of atoms or molecules increased which resulted in higher deposition rate [24].

IJSER

2. 8 References

[1] Q. Sun, Y. Wang, X. Yuan, Y. Li, J. Yang, H. Jin, F. Li, Superlattices and microstructures 64 (2013) 535

[2] S.K. Lee, J.Y. Son, Appl. Phys. Lett. 100 (2012) 132109

[3] M.S. Kim, S. Kim, J.Y. Leem, Appl. Phys. Lett. 100 (2012) 252108

[4] P.S. Venkatesh, V. Ramakrishnan, K. Jeganathan, Mater. Research Bulletin 48 (2013) 3811

[5] M. Thomson, J.L. Hodgkinson, D.W. Sheel, Surface & Coatings Technology 230 (2013) 190–195

[6] M. Asghar, K. Mahmood, M-A Hasan, Key Eng. Research 512 (2012) 132

[7] C-L Zhang, W-N Zhou, Y. Hang, Z. Lu, H-D Hou, Y-B Zuo, S-J Qin, F-H Lu, S-L Gu, J. Crystal Growth 310 (2008) 1819

[8] J. Zhao, L. Hu, Z. Wang, Z. Wang, H. Zhang, Y. Zhao, X. Liang, J. Crystal Growth 280 (2005) 455

[9] X.L. Zhang, K.N. Hui, K.S. Hui, J. Singh, Materials Research Bulletin 48 (2013) 1093–1098

[10] S. Nicolay, M. Benkhaira, L. Ding, J. Escarre, G. Bugnon, F. Meillaud, C. Ballif, Solar Energy Materials & Solar Cells 105 (2012) 46–52

[11] A.Y. Cho, F.K. Reinhart, J. Appl. Phys. 45 (1974) 1812

[12] W.C. Hughes, W.H. Rowland, Jr., M.A.L. Johnson, S. Fujita, J.W. Cook, J.F. Schetzina, J. Ren. J.A. Edmond, J. Vac. Sci. Technol. B 13 (1995) 1571

[13] O. Bierwagen, M.E. White, M-Y Tsai, J.S. Speck, Molecular Beam Epitaxy (2013) 347

[14] Y.S. Park, M.S. Seo, J.S. Kim, J. Lee, Materials Research Bulletin 48 (2013) 5136–5140

[15] X-Ray Diffraction, A Report For the 2004 Nanotechnology Teachers Workshop, The University of Tulsa, Pamela Diaz.

[16] Encyclopedia of materials characterization, C. Richard Brundle and Charles A. Evans, Jr.

IJSER

[17] Characterization of materials, Elton N, Kaufmann, Wiley-interscience

[18] D.V. Lang, J Appl. Phys 45 (1974) 3025

[19] G.L. Miller, J.V. Ramirez, D.A.H. Robinson, J. Appl. Phys 46 (1975) 2638

[20] L.C. Kimerling, IEEE Trans. Nucl. Sci, NS-23 (1976) 1497

[21] J-C Chang, J-W Guo, T-P Hsieh, M-R Yang, D-W Chiou, H-T Cheng, C-L Yeh, C-C Li, S-Y Chu, Surface & Coatings Technology 231 (2013) 573–577

[22] M Asghar, K Mahmood, Faisal Malik, M A Hasan, J. Phys:Conference Series 439 (2013) 012031

[23] G.A. Kumar, M.V.R. Reddy, K.N. Reddy, IEEE Xplore 978 (2011) 4673

[24] K-S Kim, H. W. Kim, C.M. Lee, Materials Science and Engineering B 98 (2003) 139

IJSER

Chapter 3 Structural and Optical Properties

3.1 Structural Properties

ZnO is II-VI compound semiconductor which crystallize in either cubic zinc blende or hexagonal wurtzite (Wz) structure where each anion is surrounded by four cations at the corners of a tetrahedron, and vice versa [1]. Under ambient conditions, the thermodynamically stable phase is that of wurtzite symmetry. The wurtzite structure has a hexagonal unit cell with two lattice parameters a and c in the ratio of c/a ratio 1:633. The structure is composed of two interpenetrating hexagonal close packed (hcp) sublattices, each of which consists of one type of atom displaced with respect to each other along the threefold c-axis by the amount of u 0.375 (in an ideal wurtzite structure) in fractional coordinates [2].

In this chapter, we have investigated the effect of Zn/O contents ratio, annealing temperature and annealing environment on the structural properties of MBE grown ZnO on Si (100) substrate. ZnO has hexagonal structure where all the octahedral sites in ZnO are empty. These empty sites are occupied preferably by the rich contents and/or point defects during the growth. Keeping this aspect of ZnO structure in view, we deliberately set the growth condition for the samples such that Zn-contents should be purposefully higher. Four samples chosen for this study with Zn/O ratio of 1.08, 1.12 and 1.22 (referred as sample A, B, C and D) confirmed by EDAX measurements shown in fig. 10

IJSER

Figure 9 Lay out of work carried out in chapter 3

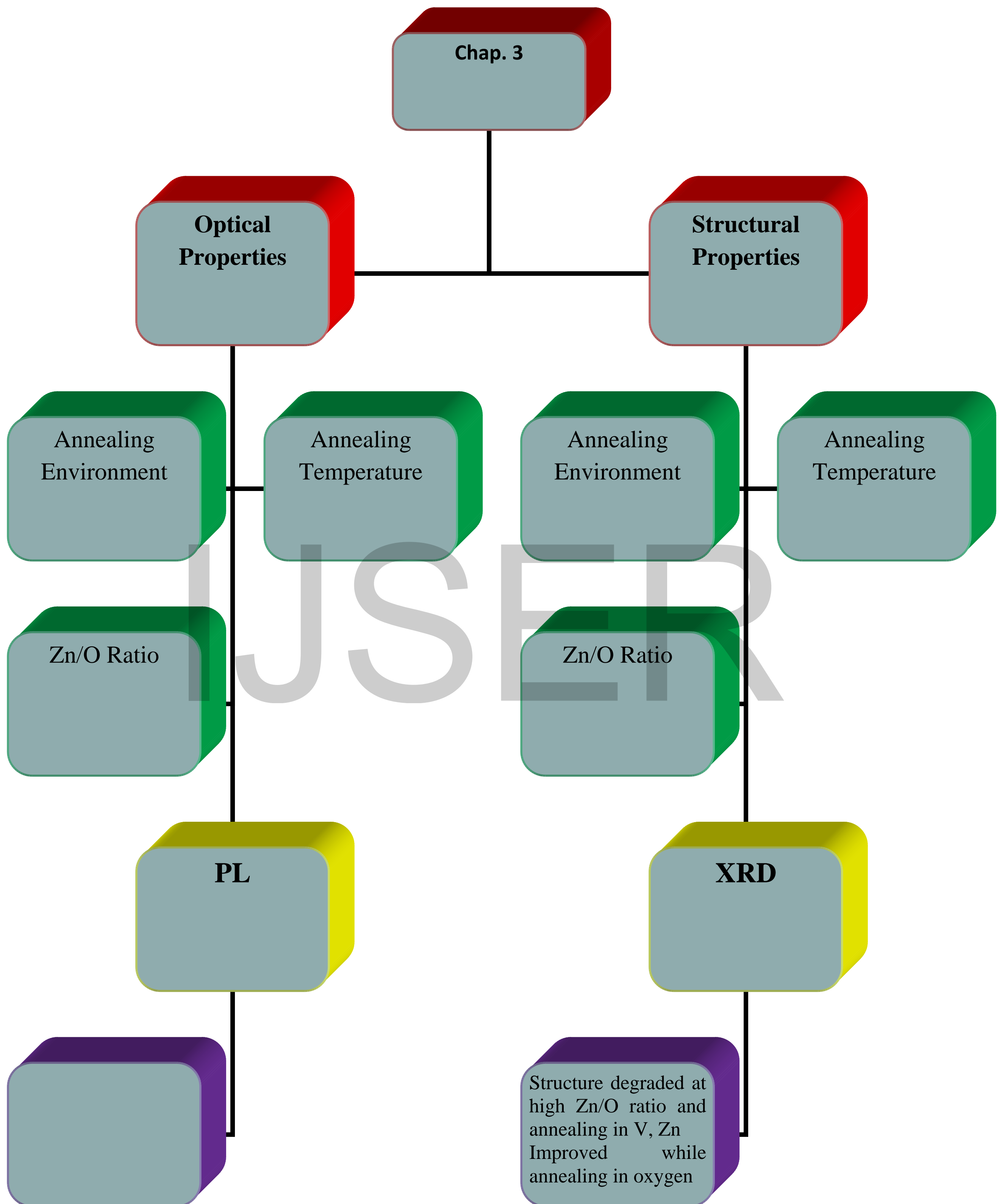

IJSER

3.1.1 Effect of Zn/O Contents Ratio

The four samples chosen for this study having At percent of Zn/O 52/48%, 53/47%, 54/46% and 55/45% and referred as D, C, B and A respectively, by molecular beam epitaxy. The concentrations for all samples were confirmed by EDX measurements as shown in fig. 10. The graph is evident that the ratio of Zn/O is 1.08, 1.12, 1.17 and 1.22 respectively.

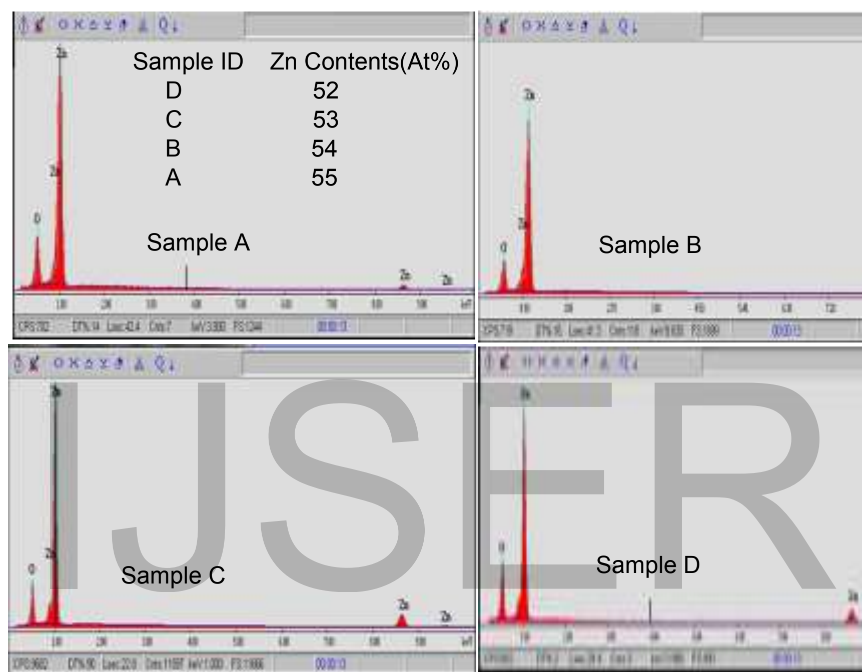

IJSER

Figure 10 EDX measurements of MBE grown ZnO with different Zn/O contents ratio

Fig. 11 shows the spectrum shows the typical XRD pattern of MBE grown ZnO on Si (100) with different Zn/O contents ratio. The spectra consists of a peak associated with (002) plane of ZnO showing that growth is highly along c-axis [3, 4]. It is evident from graph that intensity of (002) peak is decreased with increasing Zn/O ratio also the peak position of (002) plane shifted towards lower angle. The standard position of ZnO (002) plane is 34.4^0, reported by many authors in the literature [5-7].

IJSER © 2017
http://www.ijser.org

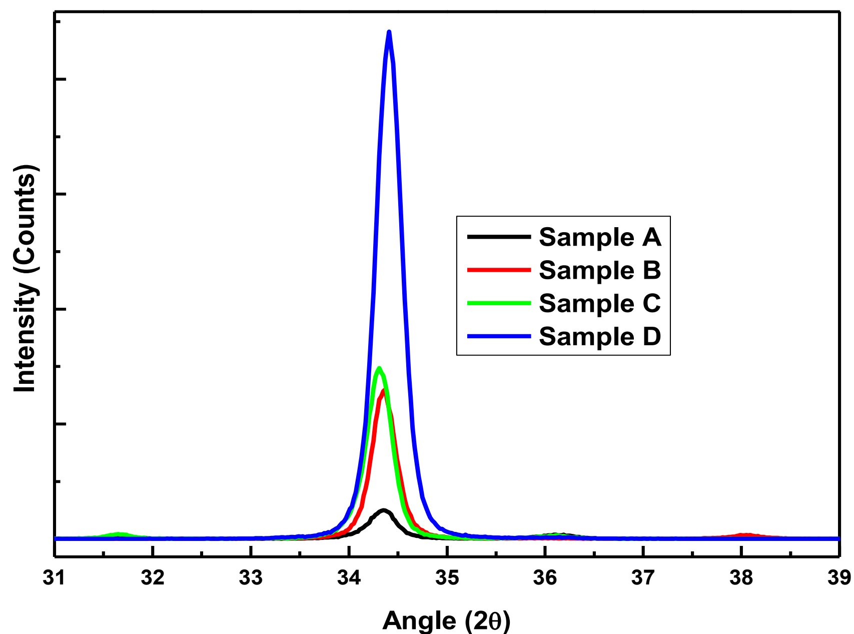

Figure 11 XRD spectra of MBE grown ZnO on Si (100) substrate with varying Zn/O contents ratio. The intensity of (002) peak decreased with increasing Zn/O ratio

The shifting of peak towards lower angle, also decreasing trend in intensity with increasing Zn/O ratio suggested that the quality of structure degraded. The possible reason of observed results may be the introduction of intrinsic donor complex defects with increasing Zn/O contents ratio.

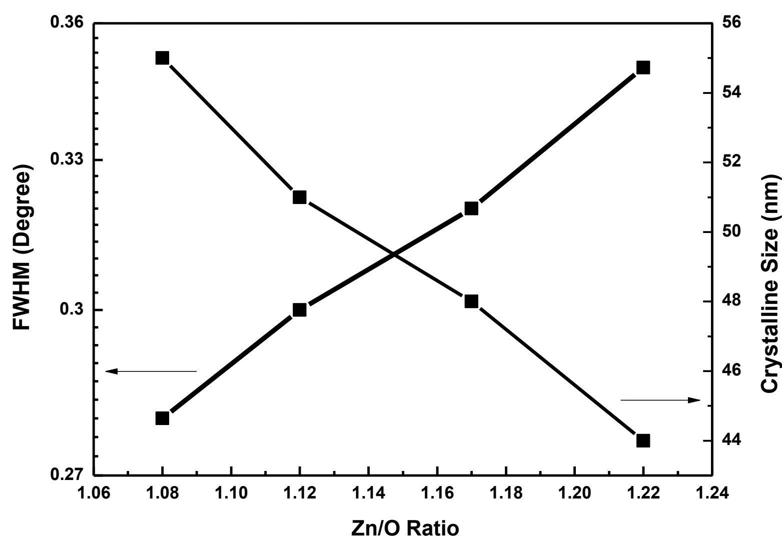

Figure 12 Effect of Zn/O ratio on FWHM of (002) plane and crystallite size of MBE grown ZnO

IJSER

Figure 12 shows the relation of FWHM and crystallite size with Zn/O ratio in the samples. The FWHM of ZnO (002) peak for samples A, B, C and D is 0.35^0, 0.32^0, 0.30^0 and 0.280^0 respectively, showing the good crystallinity of films. We observed that with increasing the Zn/O ratio in the samples, the FWHM of samples increases and crystallite size decreases. This means that the crystalline quality degrades with the increase of Zn/O ratio in the samples. The degradation of crystalline quality strongly supported our argument that increase in Zn/O contents ratio probably produced both oxygen vacancies and zinc-interstitials that can form a complex and degrades the crystal quality.

3.1.2 Effect of annealing Temperature

The density of intrinsic defects was also modulated by annealing samples in oxygen environment for one hour in the temperature range 500 to 800 ^{0}C.

IJSER

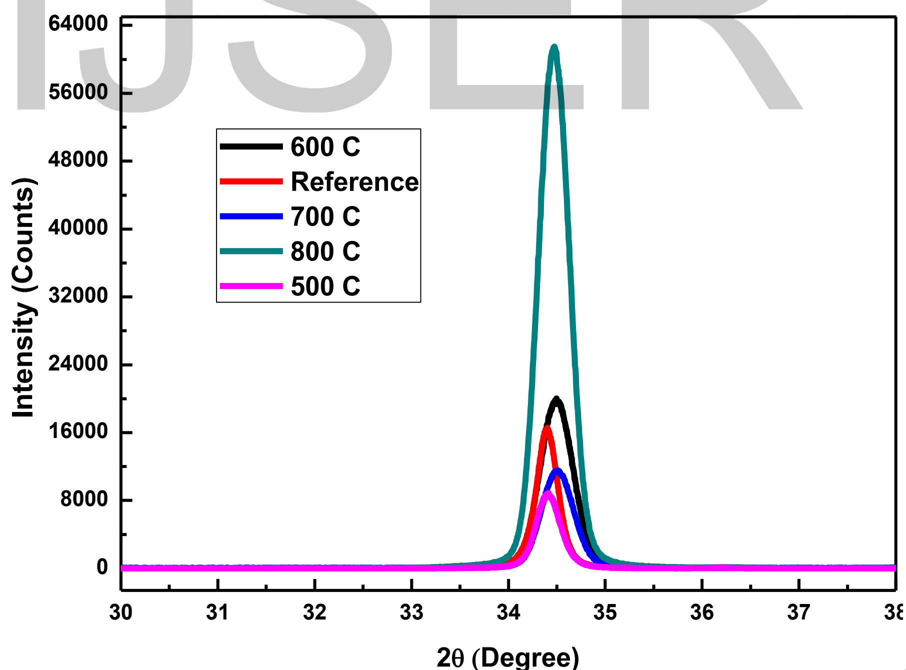

Figure 13 XRD spectrum of MBE grown ZnO on Si substrate annealed in oxygen environment for one hour at different temperature

Fig. 13 is a typical XRD spectrum of MBE grown samples annealed in oxygen environment for one hour at different temperatures ranging from 500 to 800 ^{o}C. The spectrum shows that all samples have two peaks at 2theta values 34.4^{0} and 72.2^{o} and related with ZnO (002) and (004) plane respectively [8]. The (002) peak in all samples is dominant which confirmed the C-axis growth of ZnO on Si substrate. The full Width Half Maximum of (002) peak for all samples has been calculated and shown in fig. 11 and table 4.

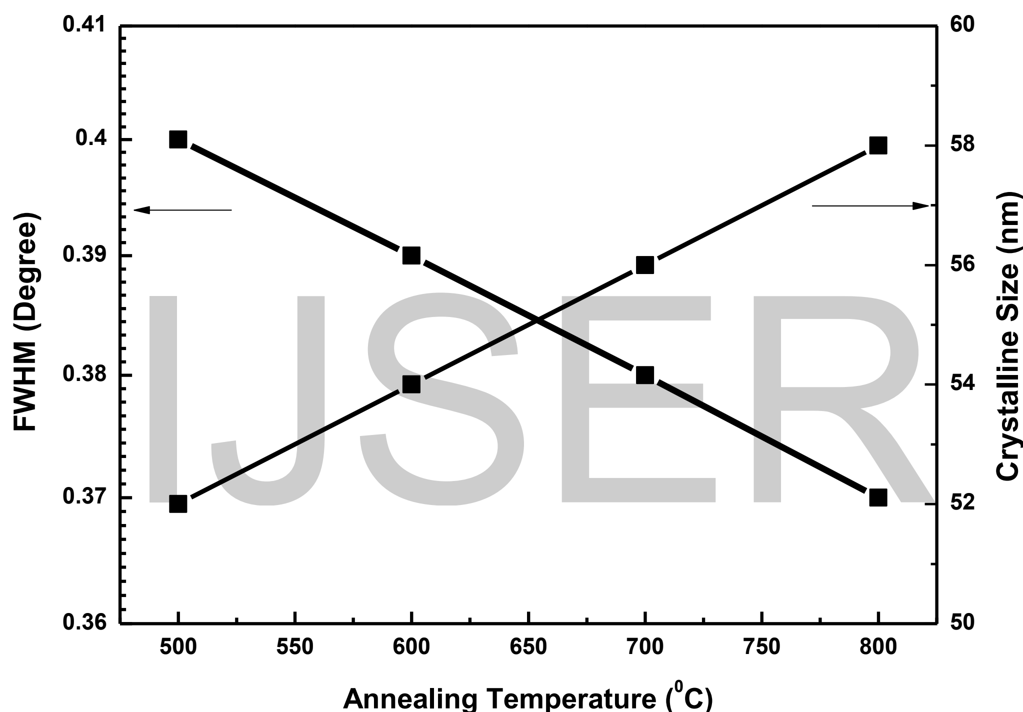

Figure 14 Relationship between FWHM of (002) plane, crystallite size and annealing temperature of ZnO grown by MBE on Si substrate

The graph demonstrated the effect of annealing temperature on the FWHM of ZnO (002) plane and crystallite size. It is evident from figure that FWHM of (002) peak deceases and crystallite size increases linearly as annealing temperature increases from 500 to 800 ^{o}C. The graph showed that FWHM decreased from 0.129 to 0.119^{o} as the annealing temperature increased from 500 to 800 ^{o}C. The decreasing trend of FWHM and increasing trend of crystallite size with annealing temperature demonstrated the improvement of crystal structure.

Table 4 Effect of annealing temperature on peak position, intensity and FWHM of (002) plane

Annealing Temp. °C	(002) Peak Position (2θ)	(002) peak Intensity (Counts)	FWHM (Degree)
Reference	34.40	16560	0.407
500	34.40	8669	0.403
600	34.90	20035	0.392
700	34.51	11525	0.387
800	34.47	61489	0.370

3.1.3 Annealing Environment Effect

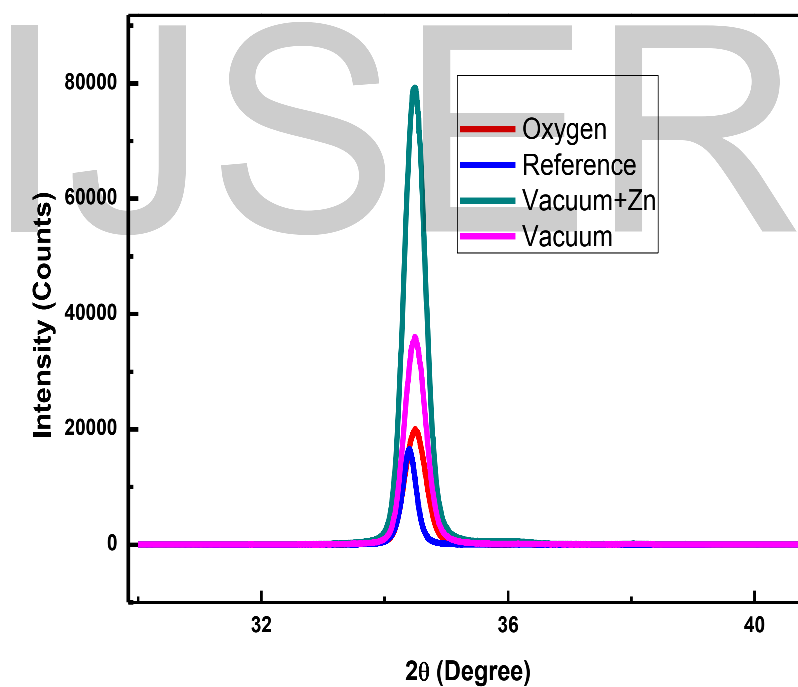

IJSER

Figure 15 Typical XRD spectrum of ZnO thin films grown by MBE and annealed in different environments for one hour

Fig. 15 is the typical XRD spectrum of MBE grown samples annealed in different environments for one hour at 600 ^{0}C. The spectrum shows that all samples have one peak at 2theta values 34.4^0

and related with ZnO (002) plane. The full Width Half Maximum of (002) peak for all samples has been calculated and shown in fig. 16 and table 5.

Table 5 Effect of annealing environment on peak position, intensity and FWHM of (002) plane

Annealing Environment	(002) Peak Position (2θ)	(002) peak Intensity (Counts)	FWHM (Degree)
Reference	34.40	16560	0.407
Oxygen	34.90	20035	0.392
Vacuum+Zn	34.48	79282	0.393
Vacuum	34.48	36072	0.402

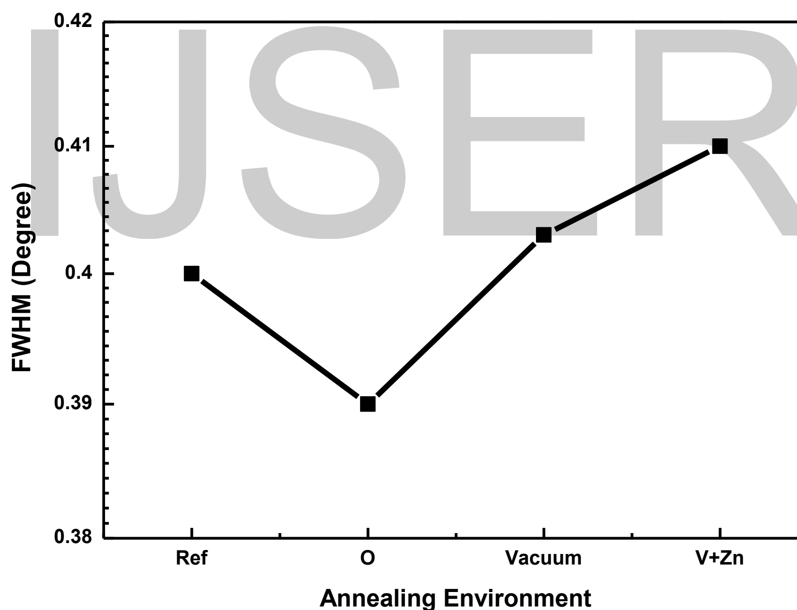

IJSER

Figure 16 Effect of annealing environment on FWHM and crystalline size of MBE grown thin films on Si substrate

Fig. 16 displayed the effect of annealing environment on the FWHM of ZnO (002) plane. The annealed in oxygen environment has smallest value of FWHM, while sample successively annealed in vacuum and zinc has largest value of FWHM. This result can be explained as; annealing in oxygen results in the reduction of defect density in the sample. But sample

successively annealed in vacuum and zinc would have large density of intrinsic defects like oxygen vacancies and zinc interstitials. Therefore decreased of FWHM while annealing in oxygen and increased of FWHM while successively annealing in vacuum and zinc is understandable.

3.2 Optical Properties

One of the unique properties of direct bandgap semiconductors that revolutionized the optoelectronics field is their ability to produce light emission in response to excitation mainly by means of electrical or optical injection of minority carriers. Light emission through any process other than blackbody radiation is called luminescence and requires external excitation as it is a nonequilibrium process. The term photoluminescence (PL), is a result of incident-photon absorption that generates electron–hole pairs and produces emission of a photon of a different wavelength. The incident photons, when absorbed, excite electrons usually from the valence band into the conduction band through momentum-conserving processes because the photon momentum is negligible. The electrons and holes thermalize to the lowest energy state of their respective bands via phonon emission before recombining across the fundamental bandgap or the defect levels within the bandgap and emitting photons of the corresponding energies.

ZnO owing to its direct band gap (3.37eV) and high exciton binding energy (60 meV) is a material of choice in optoelectronic industry [9]. The large exciton binding energy paves the way for an intense near band edge excitonic emission at room and even higher temperatures, because this value is 2.4 times the room-temperature (RT) thermal energy (kBT¼25 meV).

Generally ZnO has two types of emission; band to band emission and defect emission. The band to band emission is observe at 3.28 eV and assigned as free exciton emission [10]. The defect emission band observed between 1.9 to 2.8 eV with center at 2.5 eV and related with intrinsic

defect in ZnO [11]. As we know very little about the nature of intrinsic defects of ZnO, therefore the origin of defect emission in ZnO is not cleared yet because controversial results have been reported. Although numerous attributions of the broad PL bands have appeared in the literature, very few of them can be considered as reliable. Here are few examples of the origin of defect emission; Vanheusden et al. [12] attributed defect PL band to transitions from the deep donor level of VO to the valence band supported by many other reports in the literature, Dahan et al. [13]] proposed that Cu impurities are the main source of defect band emission in un-doped ZnO, C. Chandrinou et al. [14] observed a yellow-orange band at 580 nm and found that its intensity increases with excess oxygen, therefore they relate it with oxygen interstitials, GL band in ZnO was attributed also to VZn acceptor [15-17]], a complex defect involving Zni [18], O_{Zn} [19], and V_O [20, 21]. Therefore reliable experimental results are needed on identification of defects and defect-related transitions that can be compared with the theory.

IJSER

3.2.1 Near Band Emission

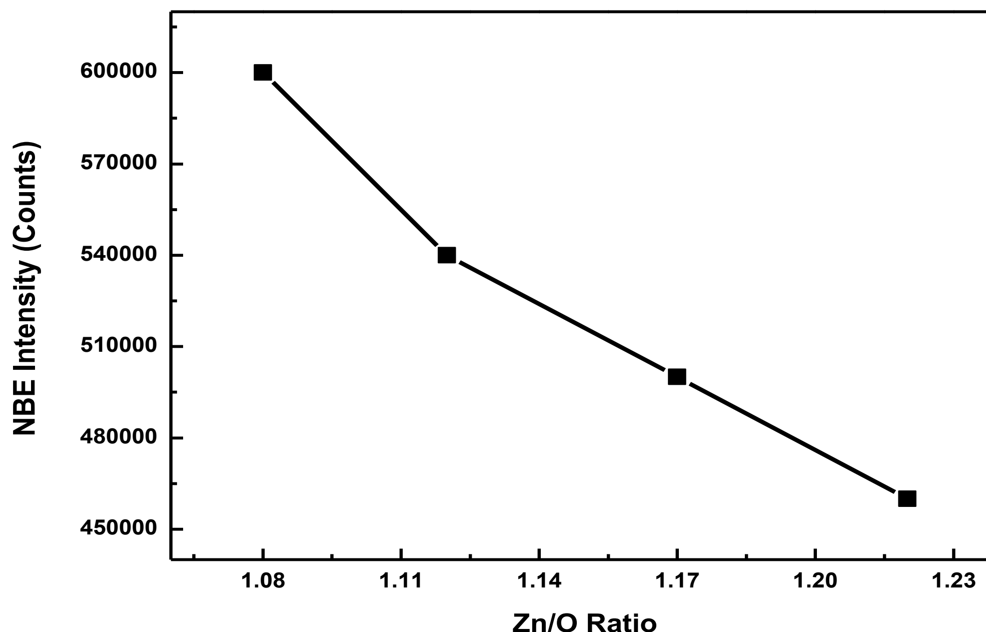

Figure 17 Effect of Zn/O ratio on the intensity of NBE of ZnO

Fig. 17 demonstrated the effect of Zn/O ratio on the intensity of PL near band edge emission (NBE) of ZnO. As a matter of fact the intensity of NBE is directly related with the concentration of intrinsic defects in the band gap of ZnO. The graph evident that the intensity of NBE PL peak decreases as the Zn/O contents ratio increases in the samples. With increasing Zn/O contents ratio, the density of defect complex V_O-Zn_i (explanation comes later) would increased. This defect complex ultimately degrades the crystal structure which in turn reduced the intensity of NBE peak.

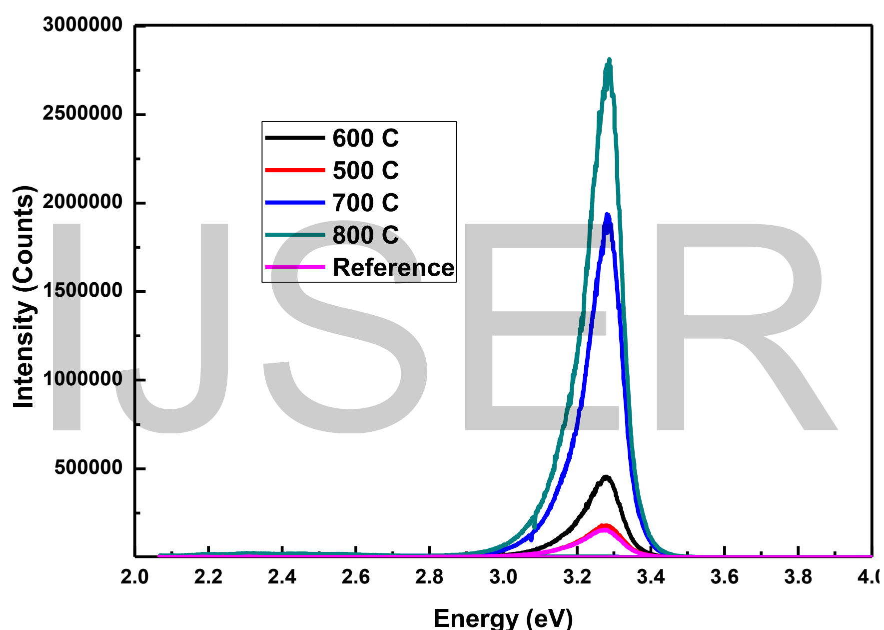

Figure 18 PL spectrum of MBE grown ZnO annealed in oxygen environment for one hour at different temperatures

Fig. above shows the typical PL spectrum of MBE grown ZnO on Si substrate and annealed in oxygen environment for one hour at different temperatures. Spectra consists of two peaks at photon energy 2.5 and 3.29 eV and related to defect emission and near band emission respectively [22, 23]. It is evident from above graph that intensity of NBE improved with annealing temperature.

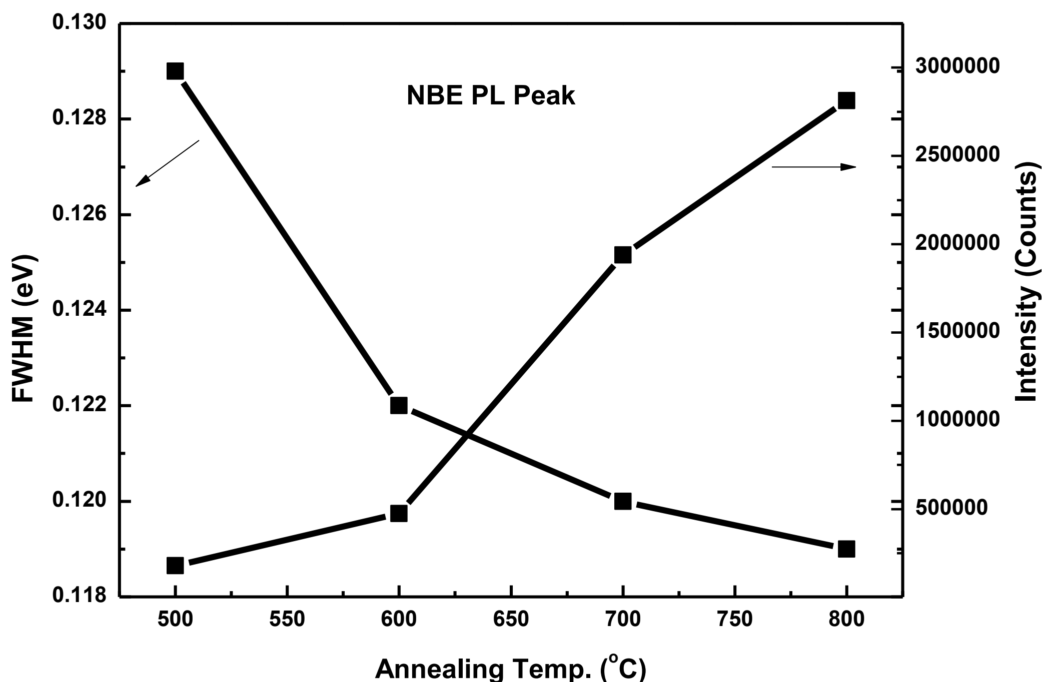

Figure 19 Graph of annealing temperature verses FWHM and intensity of PL near band edge emission of ZnO grown by MBE on Si substrate

Fig. 19 demonstrated the dependence of annealing temperature on the intensity and FWHM of near band emission. The intensity of NBE increases with annealing temperature and FWHM decreased. As a matter of fact the intensity of NBE is directly related to the crystal structure of grown film as describe by Fan et al [24]. The measured value of FWHM decreases as the annealing temperature increases from 500 to 800 ^{0}C. The result again confirmed the argument that annealing temperature improved the crystal structure by compensating the available intrinsic oxygen vacancies. Therefore the FWHM of NBE is decreased with annealing temperature.

IJSER

Table 6 Effect of annealing temperature on position of NBE, intensity of NBE, FWHM of NBE and ratio of NBE to DE of MBE grown ZnO on Si substrate

Annealing Temperature (^0C)	NBE Peak Position (eV)	NBE peak Intensity (Counts)	Peak Position DLE (eV)	Ratio of NBE to DLE peak
Reference	3.276	155830	2.30	59.43173
500	3.280	180066	2.32	24.62946
600	3.276	455614	2.32	33.87968
700	3.280	1938631	2.32	130.26683
800	3.287	2813357	2.32	120.19811

IJSER

3.2.2 Defect Emission

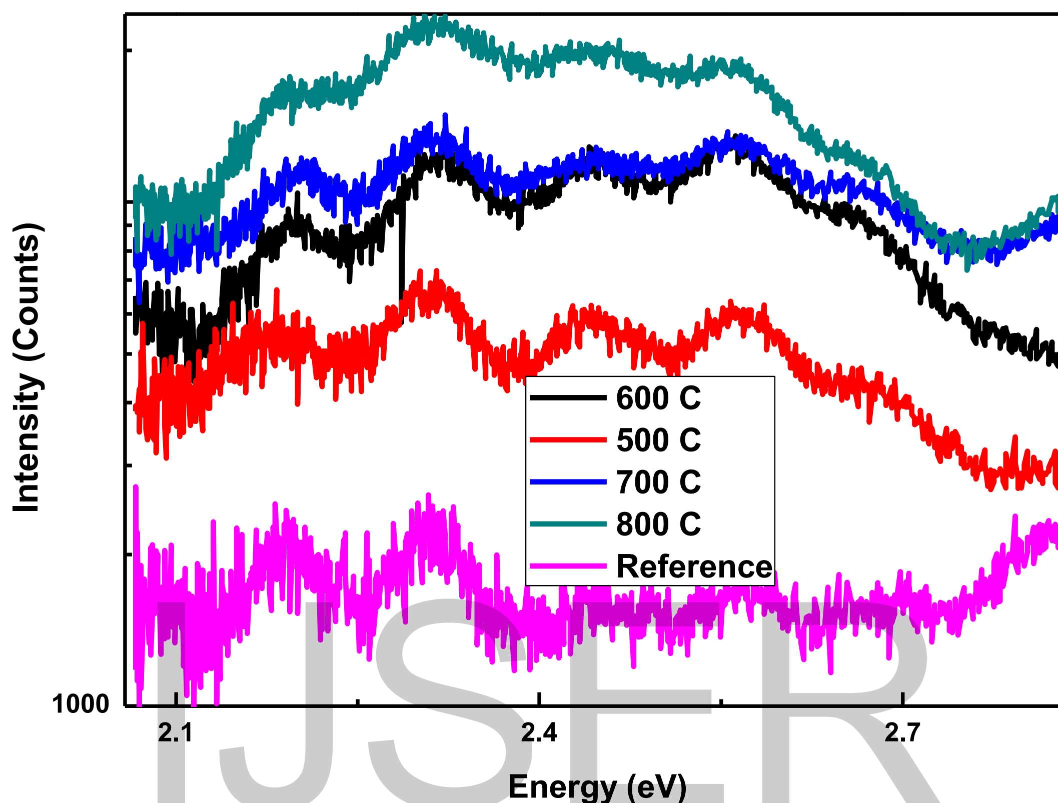

Figure 20 Typical PL spectrum of MBE grown ZnO samples annealed at different temperatures

Fig. 20 shows the defect emission spectrum of MBE ZnO samples annealed in oxygen environment for one hour at different temperatures from 500 to 800 ^{0}C, keeping a step of 100 ^{0}C. It is believed that defect emission is not related to the transition from oxygen vacancy to valance band because results presented in this dissertation not supported the argument. The defect emission increases as the annealing temperature increases from 500 to 800 ^{0}C. It is reported in literature [25] that annealing in oxygen environment fills the available oxygen vacancies due to incoming oxygen species and extra oxygen atoms go to interstitials sites to form oxygen interstitials acceptor defect. Therefore the density of oxygen vacancies becomes small at higher annealing temperatures. The enhancement of defect emission at higher annealing temperature

suggested that oxygen alone is not the source of defect emission in bulk ZnO. To investigate the real origin of defect emission, room temperature PL spectroscopy was performed of samples annealed in different environments and results are presented in fig. 21.

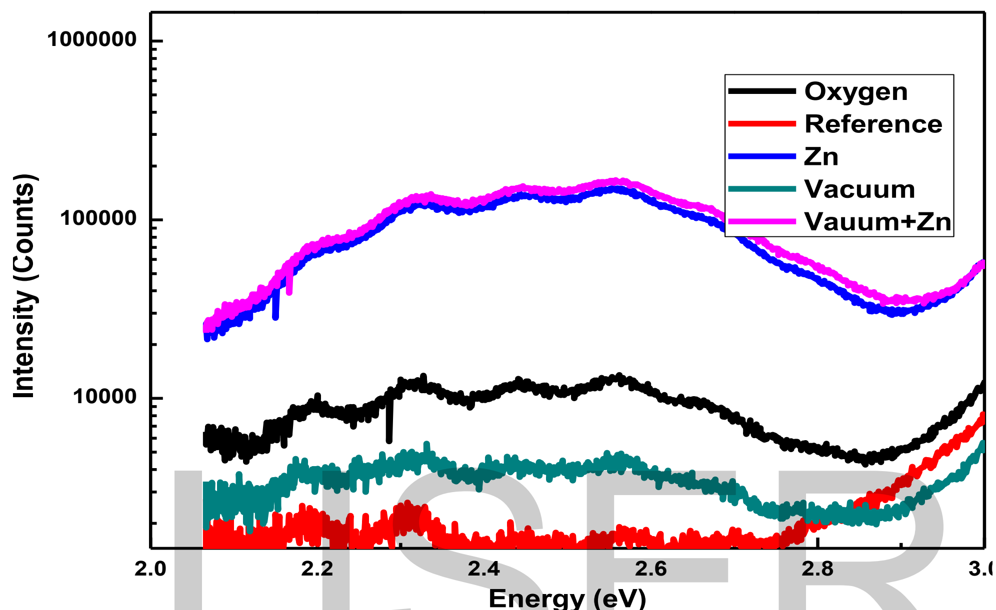

Figure 21 Typical PL spectrum of MBE grown ZnO on Si substrate annealed at 600 0C for one hour in different environments

Fig. 21 shows the typical PL spectrum of MBE grown ZnO on Si substrate and annealed in different environments for one hour. The graph shows consists of PL defect emission band having center at 2.5 eV. An interesting feature is observed that defect emission covers the whole visible range of light spectrum. The graph demonstrated that defect emission increases by annealing in different environments. A small increased is observed while annealing in vacuum and oxygen environments. But defect emission significantly enhanced while annealing in zinc and successively annealed in vacuum and zinc. It is argued that defect emission is related to transition from Zn-interstitials donor defect to O-interstitials acceptor defect. The enhancement of defect emission while annealing both in oxygen and zinc strongly suggested that transition may occurs between two intrinsic defects which results in the emission of visible photon.

Furthermore the calculated activation energies of zinc interstitials and oxygen interstitials are 0.15 and 0.72 respectively in the band gap [26, 27]. If the band gap has been taken as 3.37 eV, the transition between zinc interstitial and oxygen interstitial emits a photon with energy 2.5 eV which is exactly the same value that is observed in PL spectrum.

Table 7 Effect of annealing environment DLE peak position and DLE peak intensity of MBE grown ZnO

Annealing Environment	DLE peak position (eV)	DLE peak Intensity (Counts)
Reference	2.3	2622
Zn	2.3-2.6	150448
Oxygen	2.31-2.55	4801
Vacuum	2.17-2.56	4308
Vacuum+Zn	2.32-2.55	168332

IJSER

3.3 References

[1] Ü. Özgür, Ya.I. Alivov, C. Liu, A. Teke, M.A. Reshchikov, S. Doğan, V. Avrutin, S.-J. Cho, H. Morkoç, J. Appl. Phys. 98, (2005) 041301

[2] Zinc Oxide; Fundamentals, Materials and Device Technology, Hadis Morkoç, Ümit Özgür, 2009 WILEY-VCH Verlag GmbH & Co. KGaA, Weinheim

[3] S. Kumar, K. Asokan, R.K. Singh, S. Chatterjee, D. Kanjilal, A.K. Ghosh, J. Appl. Pys. 114 (2013) 164321

[4] C. Xiong, R.H. Yao, W.J. Wan, J.X. Xu, Optik 125 (2014) 785–788

[5] Y-C Chen, E. Goering, L. Jeurgens, Z. Wang, F. Phillipp, J. Baier, T. Tietze, G. Schutz, Appl. Phys. Lett. 103 (2013) 162405

[6] A. Kushwaha, H. Tyagi, M. Aslam, AIP ADVANCES 3 (2013) 042110

[7] S. Talam, S.R. Karumuri, N. Gunnam, Nanotechnology 2012 (2012) 372505

[8] Y. Xu, B. Yaoa,b, Y.F. Li, Z.H. Ding, J.C. Li, H.Z. Wang, Z.Z. Zhang, L.G. Zhang, H.F. Zhao, D.Z. Shen, J. Alloys and Compounds 585 (2014) 479–484

[9] R. Yousefi, F. Jamali-Sheini, A. Sa'aedi, A. Khorsand Zak, M. Cheraghizade, S. Pilban Jahromi, N. Ming Huang, Ceramics International 39 (2013) 9115–9119

[10] Y. Wu, F. Xu, D. Guo, Z. Gao, D. Wu, K. Jiang, Appl. Surf. Sci. 274 (2013) 39–44

[11] J-C Wang, Y-T Liang, F-C Cheng, C-H Fang, H-I Chen, C-Y Tsai, J-A Jiang, T-E Nee, J. Luminescence 136 (2013) 11–16

IJSER

[12] K. Vanheusden, C.H. Seager, W.L. Warren, D.R. Tallant, J.A. Voigt, Appl. Phys. Lett. 68 (1996) 403

[13] P. Dahan,, V. Fleurov, P. Thurian, R. Heitz, A. Hoffmann, I. Broser, Journal of Physics: Condensed Matter, 10 (1998) 2007

[14] C. Chandrinou, N. Boukos, C. Stogios, A. Travlos, Microelectronics Journal 40 (2009) 296–298

[15] X. Yang, G. Du, X. Wang, J. Wang, B. Liu, Y. Zhang, D. Liu, H.C. Ong, S. Yang, J. Crystal Growth 252 (2003) 275

[16] B. Guo, Z.R. Qiu, K.S. Wong, Appl. Phys. Lett. 82 (2003) 2290

[17] H-J Egelhaaf, D. Oelkrug, J. Crystal Growth 161 (1996) 190

[18] N.O. Korsunska, L.V. Borkovska, B.M. Bulakh, L-Y Khomenkova, V.I. Kushnirenko, I.V. Markevich, J. Luminescence 102–103 (2003) 733

[19] B. Lin, Z. Fu, Y. Jia, Appl. Phys. Lett. 79 (2001) 943

[20] H.F. Leiter, H.R. Alves, N.G. Romanov, D.M. Hoffmann, B.K. Meyer, Physica B 201 (2003) 340–342

[21] H.F. Leiter, H.R. Alves, N.G. Romanov, D.M. Hoffmann, B.K. Meyer, Physica Status Solidi b: Basic Research 226 (2001) 224

[22] S. Singha, P. Chakrabart, Superlattices and Microstructures 64 (2013) 283–293

[23] C. Sui, Z. Lu, T. Xu, Optical Materials 35 (2013) 2649–2653

[24] F-B Fan, S-Y Yang, P-F Zhang, Y-H Wei, X-L Liu, C-M Jiao, Q-S Zhu, Y-H Chen, Z-G Wang, Chin. Phys. Lett. (2007) 24 2108

IJSER

[25] F. Sun, C.X. Shan, S.P. Wang, B.H. Li, Z.Z. Zhang, D.X. Zhao, B. Yao, Appl. Surf. Sci. 256 (2010) 3390

[26] S-M Lukas, L. Judith, D. MacManus, *Materialstoday* 10 (2007) 40

[27] A. Janotti and Chris G Van de Walle, Rep. Prog. Phys. 72 (2009) 126501

IJSER

Chapter 4

Conductivity Control

4.1 Introduction

To get benefits from the fruits offered by ZnO, it is essential to control the conductivity type including its polarity. ZnO is naturally an n-type semiconductor which can be easily grown by doping. Group first and group five elements are generally used as dopants for n-type ZnO, replacing Zn and O respectively.

In the literature, it is suggested that the origin of intrinsically n-type conductivity of ZnO is due to intrinsic defects [1-3], but the responsible donor is still controversial. One can find many reports in the literature about the n-type conductivity of ZnO but with wavered results. Some of the popular examples are presented here and detail can be found in table 2.

IJSER

Janotti et al [4] calculate the energy levels of native donors by first principal study (V_O, Zn_i) in ZnO and made a conclusion that none of the intrinsic defect plays a role in the n-type conductivity of ZnO. His results demonstrate that binding energy of V_O is very small in Zn-rich conditions grown samples, but it is deep donor and cannot play a role in the n-type conductivity. Lukas et al [5] proposed that in Zn-rich conditions, Zn_i defects are shallow donors and are the main source of n-type conductivity. Because in Zn-rich conditions, the extra Zn-atoms always occupy the octahedral site which is shallow one. McCluskey et al [6] were argued that hydrogen is possible candidate for the n-type conductivity in ZnO. According to them H has very small size and has high diffusion coefficient, therefore can be easily diffused into ZnO and it is present

Figure 22 Layout of Chapter 4

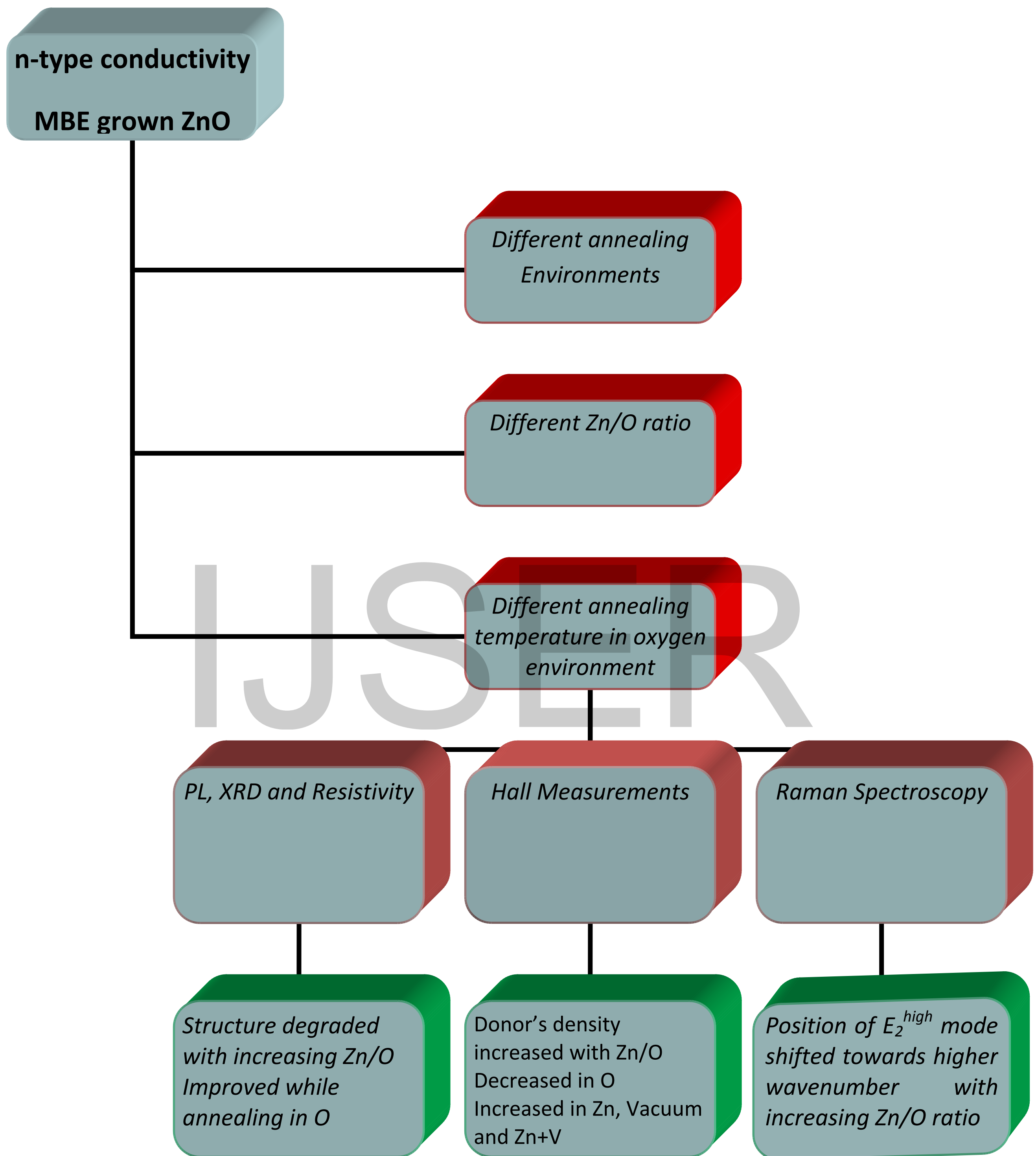

IJSER

even in high vacuum conditions. The calculated activation energy of hydrogen in ZnO is suggested that it can donate electron to the conduction band. Erhart et al [7] were in favor of V_O. They claimed that oxygen vacancy is shallow donor and may responsible for intrinsically n-type conductivity. Moreover simulation study has also been performed on the intrinsic donor nature of complexes and found that V_O-Zn_i complex, in particular, has lowest formation energy in n-type ZnO [8]. For example Y-S Kim et al [9] theoretically calculated the formation energy of V_O-Zn_i complex as a strong candidate for native shallow donor in ZnO lattice. Furthermore, D-H Kim et al [110] theoretically proposed that V_O-Zn_i complex might be the real origin of n-type conductivity of ZnO but no experimental evidence is available in the literature so far.

So after review, situation is not clear yet because we can find some contradictory results. Therefore we performed a detailed experimental study to investigate the real origin of n-type conductivity of ZnO.

IJSER

Table 8 Origin of n-type conductivity proposed by different authors

Author	Reference	Proposed origin
Janotti et al	Rep. Prog. Phys. 72 (2009) 126501	Impurities during growth
Lukas et al	Materialstoday 10 (2007) 40	Zn-interstitials
McCluskey et al	J. Appl. Phys. 106 (2009) 071101	H impurity
Erhart et al	Phys. Rev. B 73 (2006) 205203	V_O

4.2 Annealing Temperature Effect on Carrier Concentration

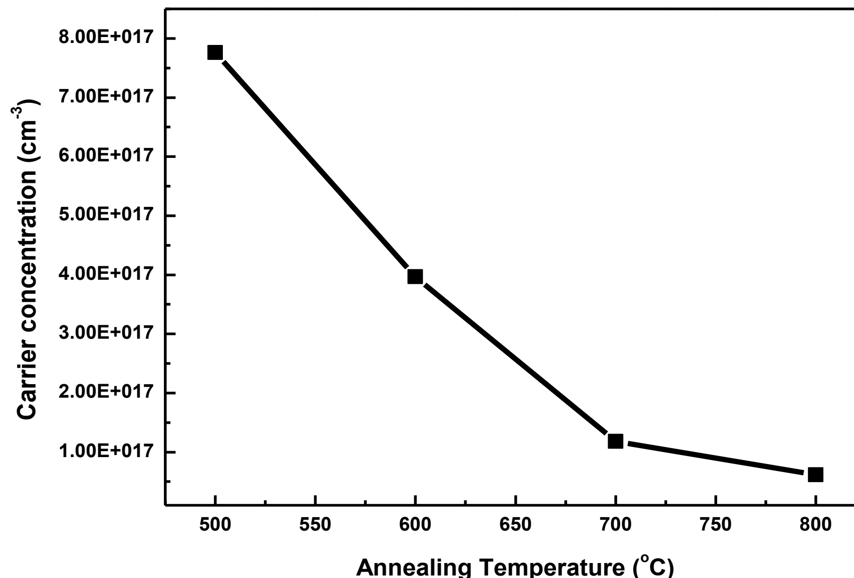

Figure 23 Dependence of carrier concentration on the annealing temperature. The carrier concentration decreases as annealing temperature increases from 500 to 8000C with step 100oC. The linear fit of 1000/T vs log Resistivity is shown in the inset

IJSER

The fig. 23 displays the effect of annealing temperature on the carrier concentration. The carrier concentration decreased from 6.23×10^{18} to 6.15×10^{16} cm^{-3} as annealing temperature increased from 500 to 800 ^{0}C. Understandably, the carrier concentration is directly related to Zn_i-V_O complex. As the concentration of this complex increases, the carrier concentration also is increased. The observed result can be explained by two-step process: (i) incoming oxygen fills V_O of V_O-Zn_i complex leaving behind Zn_i; (ii) Zn_i releases its energy and moves to a lower energy state with respect to the conduction band minima and/or occupies inactive location. This type of interaction is also demonstrated by Hadia et al [11]. The physical mechanism of Zn_i-V_O complex was explained by Y.-S. Kim et al.[10]. They theoretically proved that there is a strong interaction between two donor-like defects i.e Zn-interstitials and O vacancies. The driving force for this attractive interaction between two donors is the quantum mechanical hybridization between the electronic orbitals of their deep and shallow states, as described by [9]. This

attractive interaction results in large reduction of total energy of the system. Therefore the concentration of Zn_i-V_O complex is high enough to explain the high carrier concentration. Furthermore, literature indicates that under oxygen environment, because oxygen vacancies are supposed to be filled with the incoming oxygen and as a result, the V_O-Zn_i complex loses its identity and owing to the relevance of V_O-Zn_i complex with N_D, and subsequent decrease in N_D is acceptable which is consistent with Young-Sung Kim et al calculations. To strengthen our results, we prepared Arrhenius plot of logarithm (resistivity) as a function of 1000/T and worked out activation energy (Shown in inset of figure 3) of the intrinsic defect associated with V_O-Zn_i complex which is surprisingly happened to be the reported activation energy of V_O-Zn_i complex i.e. 1.22 eV [10]. This result confirms theoretical predictions related with V_O-Zn_i complex involvement in free carrier concentration in ZnO lattice.

4.3 Annealing Environment Effect on Carrier Concentration

On the other hand annealing of samples in Zn, vacuum and successively in Zn and vacuum environment resulted increase in N_D as shown in Table 9, which means that incoming Zn ions might have found inactive V_O to form more V_O-Zn_i complex entities in the structures. This argument is in line with the peculiar ZnO structure where a lot of space is available to accommodate foreign species [5] and hence N_D increases. Furthermore, theoretical calculations appeared in literature revealed that oxygen vacancies are deep donors in the bandgap of ZnO with lowest formation energy among the intrinsic defects in n-type ZnO. While Zn-interstitials defects are shallow donors but their formation energy in n-type ZnO is very high [12], therefore, intrinsic n-type ZnO would have high density of V_O together with a small density of Zn-interstitials. Hence small increase in carrier concentration with annealing in vacuum and about two orders increased in carrier concentration when annealed in Zn are justified.

IJSER

Table 9 Effect of annealing environment on carrier concentration, mobility and resistivity of MBE grown samples

Annealing Environment	Carrier Concentration (cm^{-3})	Mobility (cm/V.Sec)	Resistivity (Ohm cm)	Conduction Type
Un-annealed	6.23×10^{18}	0.52	1.90	N
Oxygen	3.97×10^{17}	2.397	6.55	N
Vacuum	7.89×10^{18}	6.88	1.48×10^{-1}	N
Zinc	1.56×10^{19}	23.55	1.699×10^{-2}	N
Vacuum+Zn	5.11×10^{19}	2.255	5.41×10^{-2}	N

As ZnO has hexagonal structure with half of the tetrahedral sites are occupied by Zn atom whereas all the octahedral sites are empty, hence there are plenty of sites for ZnO to accommodate intrinsic (Zn-interstitials, O-vacancy and/or Zn-antisite) [13] and extrinsic defects as well. Zinc being in larger quantity in all samples, demonstrated by EDX measurements therefore, occupy the interstitials sites referred as Zn_i. Thereafter, Zn_i form a complex with V_O and therefore the density of V_O-Zn_i complex increases with Zn/O ratio.

IJSER

4.4 Effect of Zn/O Ratio

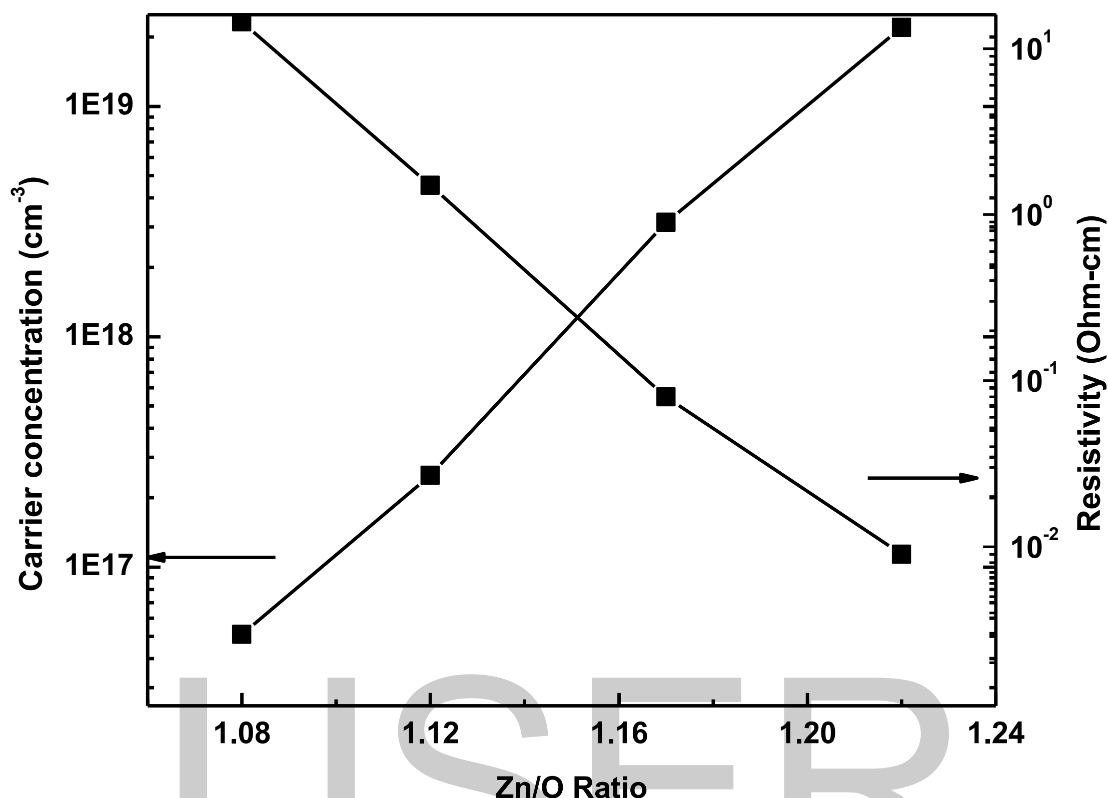

Figure 24 Effect of Zn/O ratio on carrier concentration and resistivity of MBE grown samples

The effect of Zn/O ratio on carrier concentration and resistivity of samples in the measurement range is shown in fig 24. With increasing Zn/O ratio in the samples, the carrier concentration increases and resistivity of samples decreases. The carrier concentration increased from 5.0×10^{16} cm^{-3} to 2.2×10^{19} cm^{-3} and resistivity decreased from 14.4 Ω cm to 0.009 Ω cm for samples with increasing Zn/O ratio from 1.08 to 1.22, respectively. These Zn-interstitials in combination with V_O form (V_O-Zn_i) which gives conduction electrons to conduction band, therefore carrier concentration increases significantly

4.5 Thickness Verses Resistivity

Fig. 25 displays the relationship between thickness and resistivity of samples. As thickness increases the resistivity of sample also increased. The resistivity of samples is directly related to

IJSER

the carrier concentration and the carrier concentration is result from the V_O- Zn_i defects. As the thickness of samples increased, crystanallity of films improves and the concentration of donor defects complex decreased which results in the increase of resistivity.

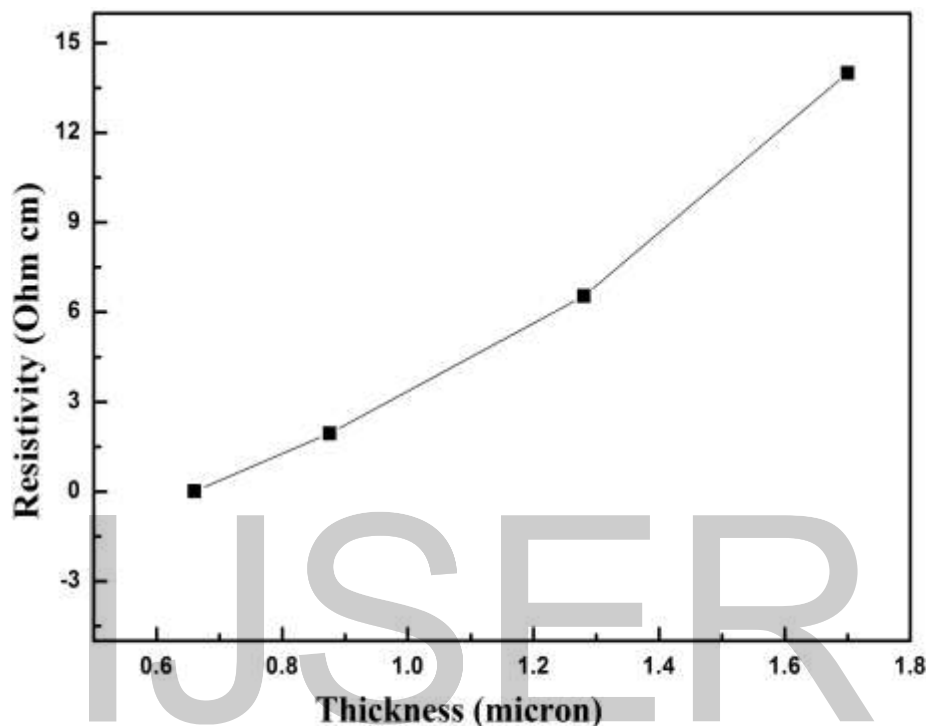

Figure 25 The graph shows the dependence of resistivity on sample thickness. Thick films have less Zn-interstitials defects and therefore have high resistivity

4.6 Raman Measurements

To support the presence of Zn-interstitials, we performed Raman spectroscopy as well. The ZnO crystal structure belongs to the space group C^4_{6v}, and the group theory analysis predicts the zone-center optical modes; A_1 + $2B_1$ + E_1 +$2E_2$. The A_1, E_1 and the two E_2 modes are Raman active, while the B_1 modes are forbidden in Raman scattering. Furthermore, the A_1 and E_1 modes are polar: their vibrations polarize the unit cell, which results in the creation of a long-range electrostatic field. This field results in the splitting of A_1 and E_1 modes into longitudinal optical

IJSER

(LO) and transverse optical (TO) components, thus creating the A_1 (LO, TO) and E_1 (LO, TO) modes.

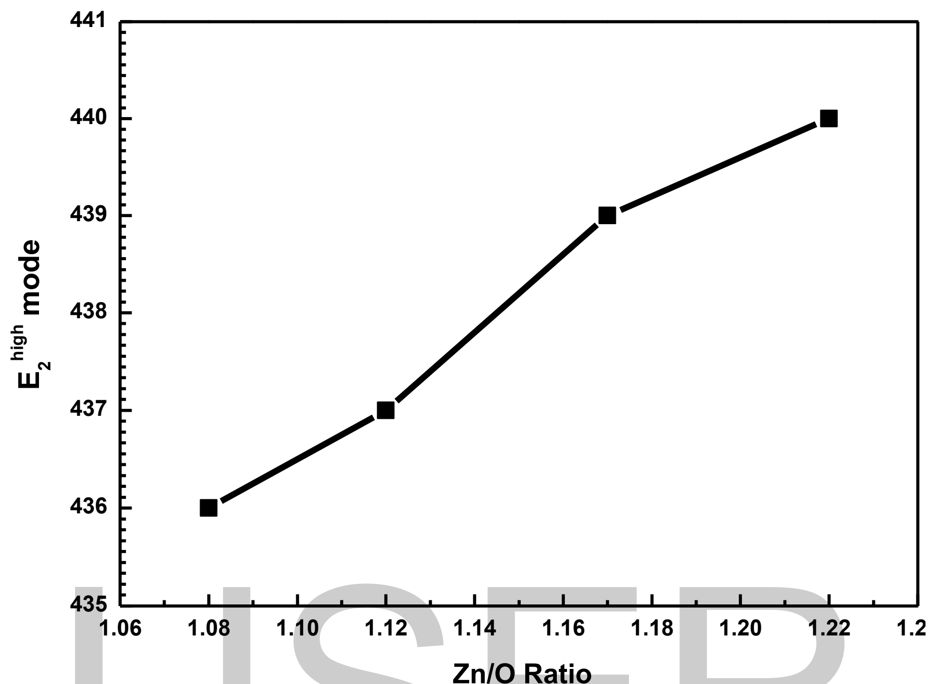

Figure 26 Fig. 5 Graph between Zn-concentration and position of E_2^{high} mode of ZnO. The experimental values exhibit shift from the theoretical values: 433. The upward shift in E2high is attributed to the presence of Zn-interstitials

Fig. 26 displays the effect of Zn-contents on the E_2^{high} Raman mode of ZnO for samples with increasing Zn/O contents ratio. The spectrum shows a non-polar optical phonon mode E_2^{high} for all samples [14]. The theoretical calculations by Tsuboi and Wada [15] predicted the frequency of E_2^{high} mode of pure ZnO to be 433 cm^{-1}. We observed this mode at 440cm^{-1}, 439cm^{-1}, 437cm^{-1} and 436cm^{-1} for samples (A, B, C and D) with Zn/O ratio 1.22, 1.17, 1.12, and 1.08 respectively. The shift of E_2^{high} phonon frequency is directly related to the stress in film. Haung et al. [16] pointed out that under a compressive stress the E_2^{high} shifts up. We observed an up shift of 7cm^{-1}, 6cm^{-1}, 4cm^{-1} and 3cm^{-1} for sample A, B, C and D respectively. This up shift indicates a

IJSER

compressive stress in the film. The reason of this stress may be excess density of V_O-Zn_i donor complex in the films.

IJSER

4.7 References

[1] F.A. Selim, H.H. Weber, D. Solodovnikov, K.G. Lynn, Phys. Rev. Lett. 99 (2007) 085502

[2] Y-S Kim, C.H. Park, Phys. Rev. Lett. Vol. 102 (2009) 086403

[3] Y-J Lin, M-S Wang, C-J Liu, H-J Huang, Appl. Surf. Sci. xxx (2010) xxx

[4] A. Janotti, Chris G Van de Walle, Rep. Prog. Phys. 72 (2009) 126501

[5] L. Schmidt-Mende, J.L. MacManus-Driscoll, Materialstoday 10 (2007) 40

[6] M.D. McCluskey, S.J. Jokela, J. Appl. Phys. 106 (2009) 071101

[7] P. Erhart, K. Albe, A. Klein, Phys. Rev. B 73 (2006) 205203

[8] R.Vidya, P. Ravindran, H. Fjellvag, B.G. Svensson, E. Monakhov, M. Ganchenkova, R.M. Nieminen, Phys. Rev. B 83 (2011) 045206

[9] K. Yong-Sung, C.H. Park, Phys. Rev. Lett. 102 (2009) 086403

[10] K. Dae-H, L. Ga-W, K. Yeong, Solid State Communications 10 (2010)1016

[11] H. Noor, P. Klason, O. Nur, Q. Wahab, M. Asghar, M. Willander, J. Appl. Phys. 105 (2009) 123510

[12] M. Asghar, K. Mahmood, A. Ali, M. Willander, I. Hussain, M-A Hasan, ECS transaction 35 (2012) 149-154

[13] X. Wang, Y.M. Lu, D.Z. Shen, Z.Z. Zhang, B.H. Li, B. Yao, J.Y. Zhang, D.X. Zhao, X.W. Fan, J. lumin. 122 (2007) 165-167

[14] C.W. Zou, H.J. Wang, M.L.Yi, M. Li, C.S. Liu, L.P. Guo, D.J. Fu, T.W. Kang, Apply. Surf. Sci. 245 (2010) 2453-2457

IJSER © 2017
http://www.ijser.org

[15] M. Tsuboi, A. Wada, J. Chem. Phys. 48 (1968) 2615

[16] Y. Huang, M. Liu, Y. Zeng, S. Liu, Mater. Sci. Eng B 97 (2003) 111

IJSER

Chapter 5 Electrical Properties

5.1 Schottky Diodes-An Introduction

To realize ZnO based devices, high quality Ohmic and Schottky metal contacts are indispensible. The performance and relaibility of these devices especially depend on the formation of insulator layer between metal and semiconductor interface, inhomogenities of Schottky barrier contacts and series resistance of diode [1-3]. Generally Schottky contacts show temperature dependent behavior as evidenced by the parameters such as ideality factor, barrier height and series resistance [4]. It is observed in the literature that I-V characteristics normally deviate from the ideal thermionic model because both ideality factor and barrier height showed strong temperature dependence behavior [5-7]. This abnormal behavior of Schottky diodes was attributed to series resistance and inhomogenites between metal and semiconductor [8, 9]. Different models have been employed to understand the abnormal behavior but the subject is still under hot debate. Different metal such as Al, Au, Ag, Pt and Pd had been used by researchers to achieve reliable Schottky contacts. These Schottky contacts have barrier heights in the range of 0.6 eV to 0.8 eV, do not seems to follow the difference in work function values, indicating the non-negligible impact of interface defect states. These interface states can be strongly depends upon the defect density of grown film and consequently on growth technique used [a]. Therefore

For electrical measurements, gold Schottky contacts with diameter 78 mm^2 were fabricated by electron beam evaporation under similar conditions.

5.2 Current-Voltage (I-V) Measurements

The thermionic emission theory for a bias voltage, V, is valid for the analysis of electrical characteristics of the Schottky barrier structures of Au/ ZnO/p-Si, and hence junction current can be expressed by [10]

IJSER

$$I = I_S\left[\exp\left(\frac{qv}{nkT}\right) - 1\right]$$

where n is the ideality factor and I_S is the reverse saturation current given by,

$$I_S = AA^*T^2 \exp\left[\frac{-q\phi}{kT}\right]$$

where A is diode area, A^* is Richardson's constant, q is charge, Φ_{ap} is apparent barrier height, k is Boltzmanns constant and T is temperature.

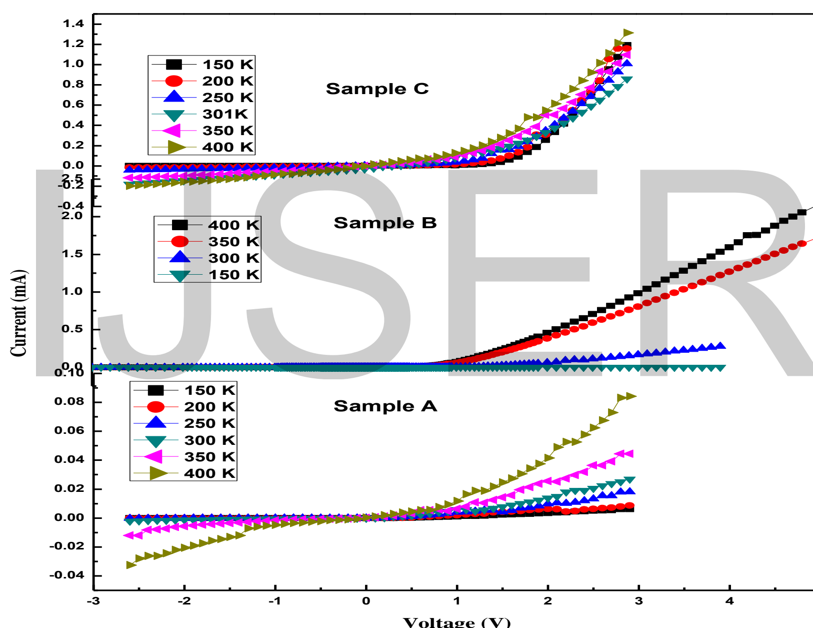

Figure 27 Temperature dependent Current-Voltage characteristics of Au/ZnO/Si Schottky diodes from 150 to 400 K for samples with different Zn/O ratio

The graph above demonstrated that Schottky behavior of contacts degrades as the Zn/O ratio increased in the samples. The turn on voltage for diodes with higher density of intrinsic defects is higher.

5.2.1 Ideality Factor

The ideality factor (n) of Schottky barrier is an important parameter that explains the perfection of metal-semiconductor junction. It is determined from the slope of semilog I-V characteristics in the exponential region (inset Fig 2) by the relation;

$$n = \frac{q}{kT \times slope}$$

Where q is the charge (C), k is Boltzmanns constant (J/K), T is Temperature (K) [11].

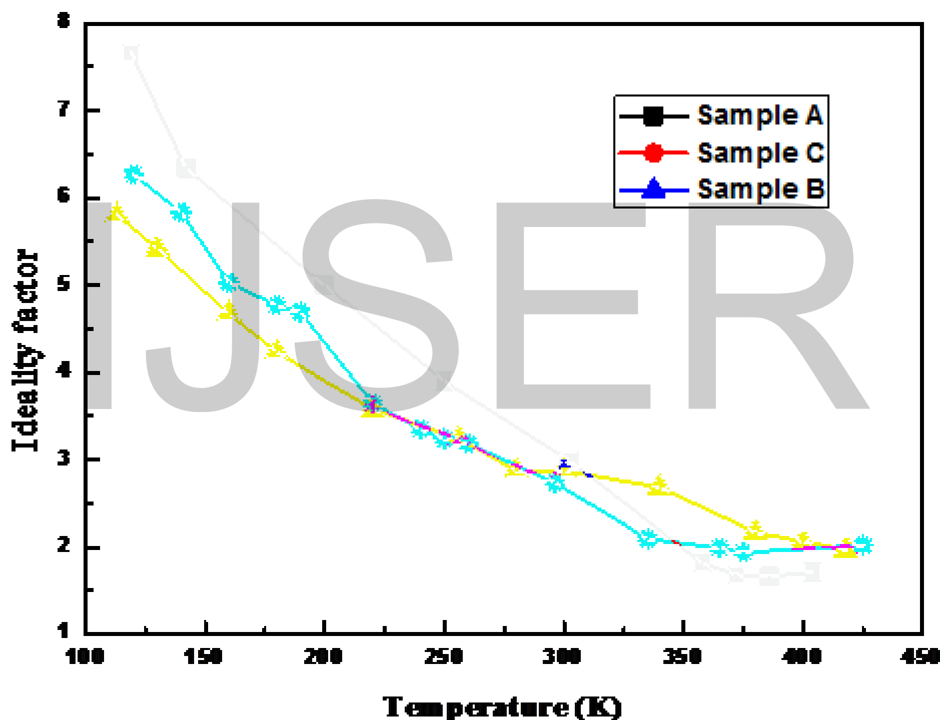

Figure 28 Effect of temperature on ideality factor of Au/ZnO/Si Schottky diodes fabricated on different samples

The measured values of ideality factor at room temperature for Au Schottky diodes fabricated on ZnO for samples A, B and C are 3.2, 3 and 2.9 respectively. The high values of n can be attributed to effects of the bias voltage drop across the interfacial layer, series resistance and inhomogeneous barrier heights [12-14]. It is also evident from this plot that room temperature

value of ideality factor for sample A is larger as compared to sample B and C. The possible reason of is that sample A has high density of surface defects, therefore would has high density of interface states.

5.2.2 Barrier Height

The barrier height is an electrostatic barrier to the charge transfer across the metal/semiconductor interface, and is denoted by Φ_B. The Φ_B can be written as [15]

$$\phi_{B(I-v)} = \frac{kT}{q}\ln\left(\frac{AA^{*}T^{2}}{I_S}\right)$$

where k is Boltzmanns constant (J/K), T is temperature (K), q is charge of electron (C), A is Schottky contact area (cm^2), A^* is Richardson constant (J/cm^2K) and Is is reverse saturation current (A).

IJSER

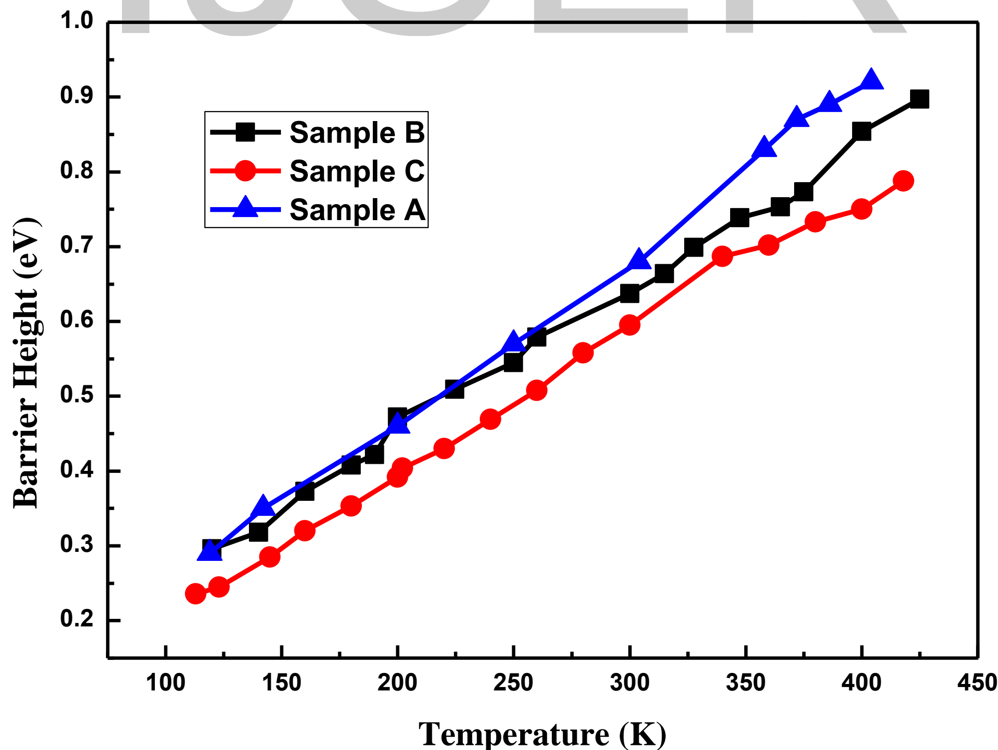

Figure 29 Effect of temperature on the barrier height of Au/ZnO/Si Schottky diodes for different samples

The barrier height (Φ_B) can be determined by the intercept of the linear part of the forward bias voltage at exponential region as shown in fig 26. The plot of temperature versus barrier height $\phi_{B(I-\nu)}$ at the temperature 150 to 400K is shown in figure 28. Like the ideality factor, $\phi_{B(I-\nu)}$ is also seemed to be a strong function of temperature. This is attributed to the fact that ZnO readily forms interfacial layer of thickness of one to two monolayer on its surface which is resulted in the existence of abundant surface states on ZnO [16].

5.2.3 Richardson Plot

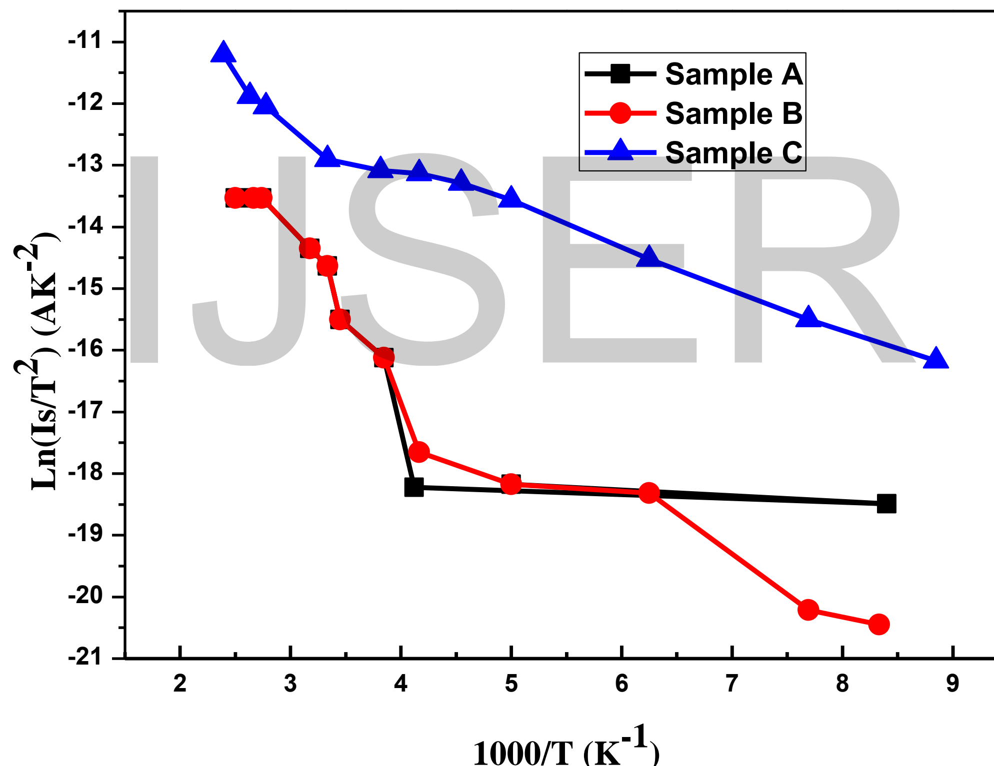

Figure 30 Richardson plot for Au ZnO/Si Scottky diode in the temperature range 150-400K for sample A, B and C

Fig. 30 show the Richardson plot for the temperature range 150-400K. The value of Richardson constant was found to be 10, 13 and 18 $AK^{-2}cm^{-2}$ for samples A, B and C respectively. The deviation of Richardson constant from the theoretical value, 32 $AK^{-2}cm^{-2}$ is due to the barrier

height inhomogenity effect. The larger deviation of Richardson plot for sample A is justified the fact that intrinsic defects play a critical role in the inhomogenity of Schottky barrier. The barrier height consists of low and high barrier area at interface. Due to these potential fluctuations at the interface, the current of diode will flow preferentially through the lower barriers in the potential distribution [17].

5.2.4 Barrier Height Inhomogenity

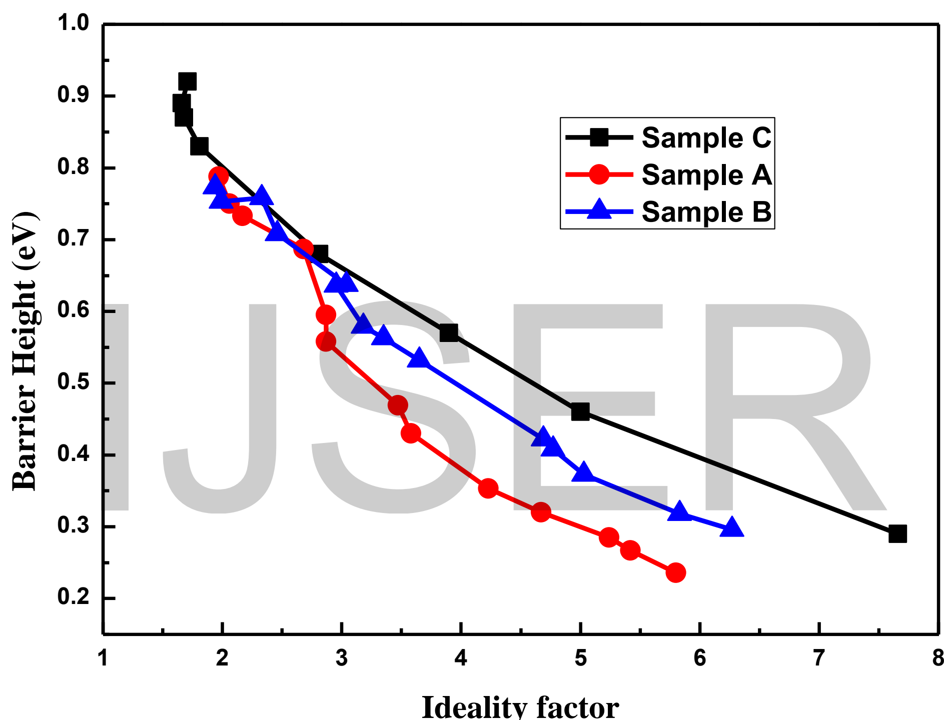

Figure 31The plot between barrier height and ideality factor. The linear relationship demonstrated the presence of inhomogenity in barrier height

The barrier height inhomogenity can be also determined by plotting the graph between ideality factor and barrier height [18]. Fig. 31 shows a plot of experimental BH and ideality factor. Fig. 31 demonstrated a linear relationship between experimental BH and ideality factor and is explained by lateral inhomogenities of BH in the schottky diode. The extrapolation of experimental BH verses ideality factor plot of n=1 has given homogenious barrier height of 1.1,

1.3 and 1.4 eV for samples C, B and A respectively. Therefore decreased of ideality factor and increased of barrier height at high temperature clearly demonstrate that there is discontinuity at Au/ZnO interface.

This barrier height inhomogeneity can be explained by using Gaussian distribution model of barrier height. According to this model the expression of barrier height can be written as [19, 20]

$\Phi_{ap}=\Phi_{bo}-q\delta_s^2/2kT$

where Φ_{ap} is the apparent BH which can be measured experimentally, Φ_{bo} is the mean BH and δ_s is the standard deviation of the BH distribution. The standard deviation is the measure of barrier height inhomogenity.

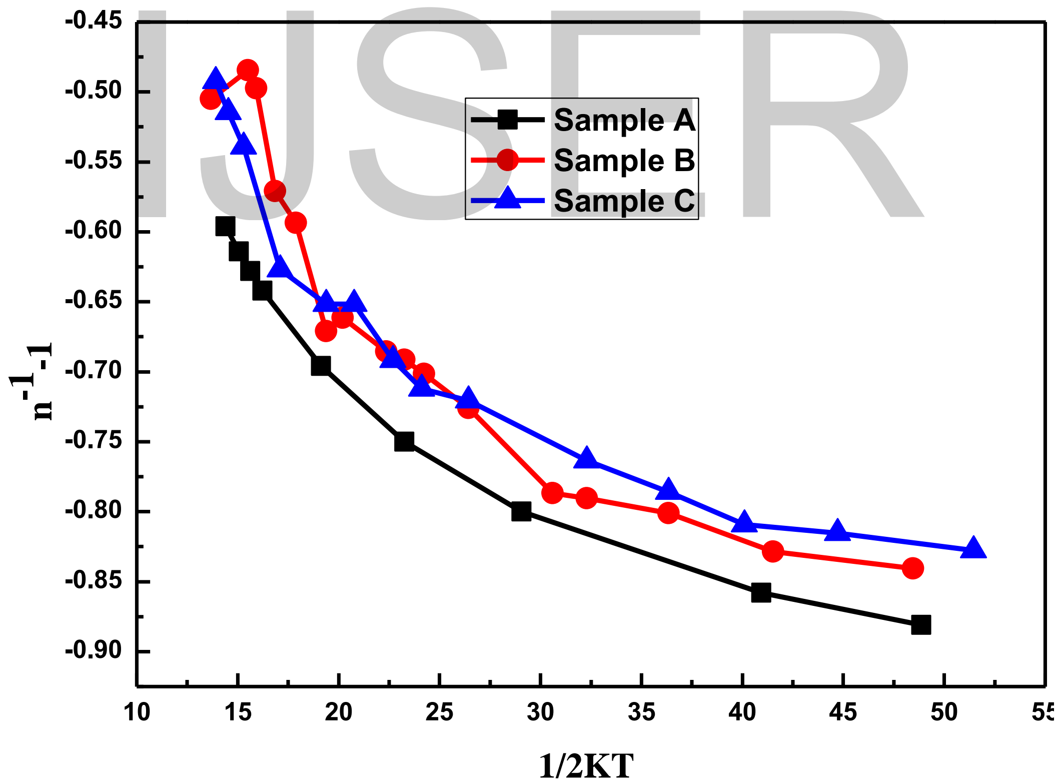

Figure 32Zero bias ideality factor verses1/2kT curves of Au/ZnO/Si Schottky diodes according to the Gaussian barrier height

The temperature dependence of δ_s is usually small and can be neglected. In this model the observed variation of ideality factor with temperature is given by [21]

$$(1/n_{ap} -1) = - \rho 2 + q\, \rho 3/2kT \quad \textbf{(6)}$$

where n_{ap} is the apparent ideality factor and ρ2 and ρ3 are voltage coefficients which may depend on temperature and they quantify the voltage deformation of the BH distribution

Again, the plot of n_{ap} versus 1/2kT should be a straight line that gives voltage coefficients ρ2 and ρ2 from the intercept and slope, respectively (Fig. 32). The values of ρ2 = 0.55 and ρ3 = -0.006 V were obtained from the experimental n_{ap} versus 1/2kT plot (Fig. 5). As the inhomogenity of the interface is depend upon the value of δ_s. The lower value of δ_s corresponds to more homogeneous barrier heights.

IJSER

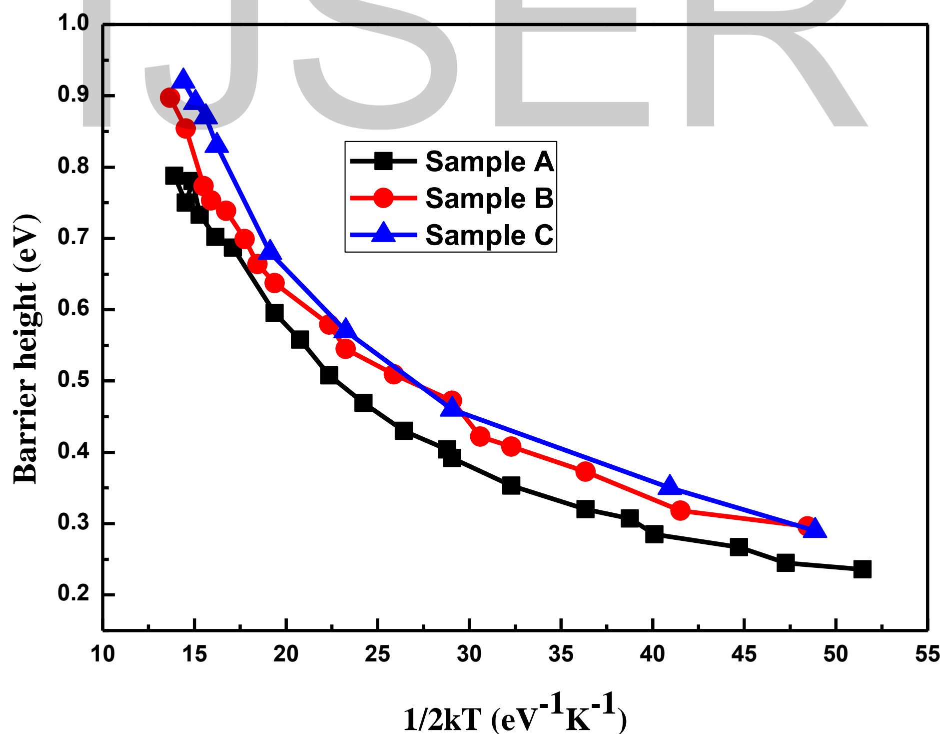

Figure 33Zero bias barrier height verses1/2kT curves of Au/ZnO/Si Schottky diodes according to the Gaussian barrier height

The linear relationship between barrier height and 1/2kT shows an agreement with current model that confirmed the discontinuity at metal and semiconductor interface. The fig. 33 shows a plot between Φ_{ap} and 1/2kT for Au/ZnO Schottky diode. The intercept and slope of this plot gives the mean barrier height and the zero-bais standard deviation with values 1.1 eV and 0.02 eV respectively.

5.3 Capacitance-Voltage (C-V) Measurements

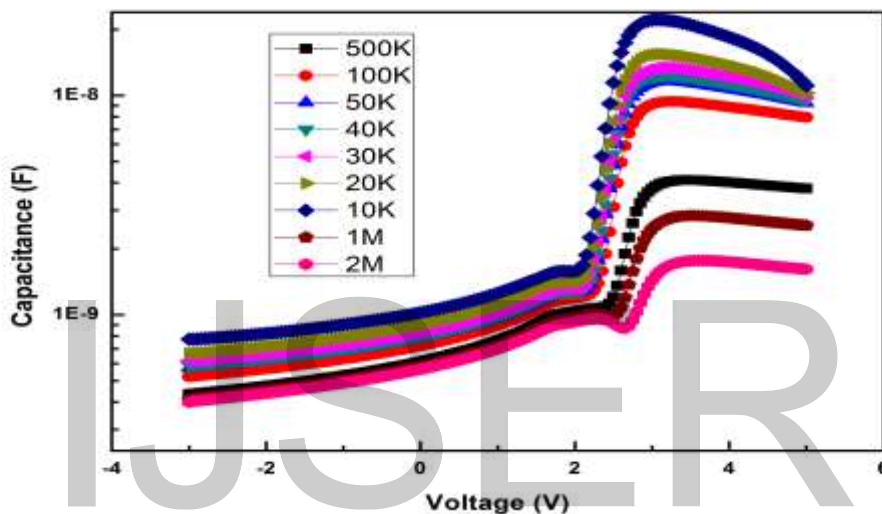

IJSER

Figure 34 Plot of C-V of Au/ZnO/Si Schottky contact at different frequencies

Fig. 34 is typical C-V characteristics of Au/ZnO/Si Schottky diode between voltage range of -4 V to +5 V at room temperature and at different frequencies ranging from 10 KHz to 2 MHz. The graph shows that the value of capacitance is decreasing with increasing frequency and plot exhibit a peak in positive voltage. This peak is gradually disappeared as frequency increased from 10 KHz to 2 MHz. The possible reasons of this peak may the presence of deep states in the band gap, series resistance and interface density states.

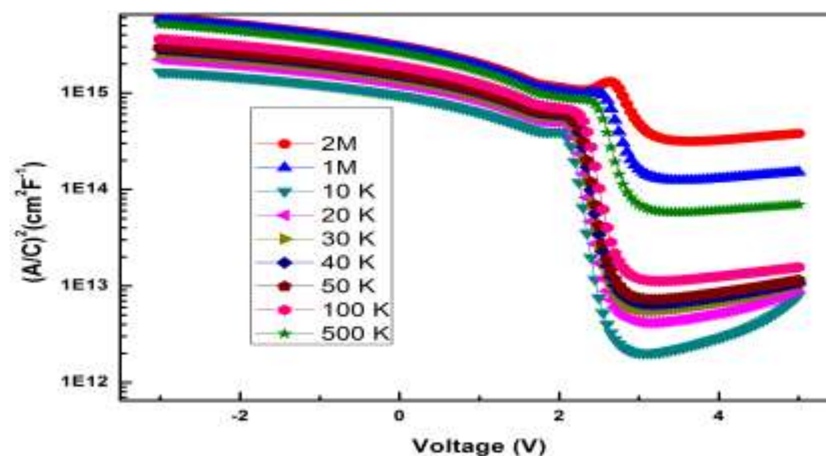

Figure 35 C^{-2}-V characteristics of Au/ZnO/Si Schottky diode at different frequencies

C–V characteristics can be analyzed by plotting $1/C^2$ vs V and deducing N_d from the slope and V_{bi} from the intercept of reversed biased capacitance-voltage (C-V) characteristics using following equation.

IJSER

$$N_d = \frac{-2}{q\varepsilon_0\varepsilon_r \frac{d\left(A/C\right)^2}{dv}}$$

Where q (1.6×10^{-19} C) is the charge on an electron, ε_o (8.85×10^{-14}) is the permittivity of the free space, ε_r (=9.66) is the relative permittivity of the medium, A is the area of the Schottky contact ($0.034cm^2$) and C is the capacitance in pF.

The measured value of doping concentration at 2 MHz frequency is 1.4×10^{16} cm^{-3}. The barrier height value can also be deduced from this graph. The barrier height obtained from reversed biased $(A/C)^2$ graph is 0.91 at 1 MHz frequency. The measured value of barrier height from C-V characteristics is high as compared to barrier height extracted from I-V data. This difference is due to the presence of interface states at interface and other possible reasons may be barrier height inhomogenity and image force lowering [22].

5.3.1 Frequency verses Capacitance

Generally the capacitance measured for the rectifying contact is dependent on the reverse bias voltage and frequency. Its voltage and frequency dependence is due to the particular features of a Schottky barrier, impurity level, high series resistance, interface states and interface layer between Au and ZnO.

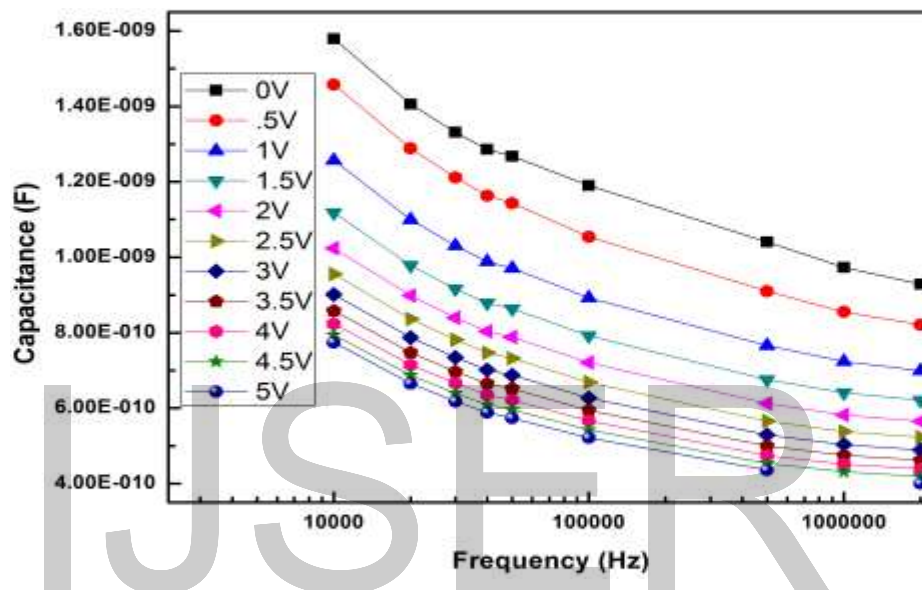

Figure 36 Frequency dependent plot of capacitance of Au/ZnO/Si Schottky diode at different biases

This dependence of capacitance on frequency is shown in fig. 5. The higher values of capacitance at low frequency are due to the excess capacitance resulting from the interface states in equilibrium with the n-type ZnO that can follow the ac signal. At low frequency the measured capacitance is dominated by the depletion capacitance of the rectifying contact, which is bias-dependent and frequency-independent. As the frequency is increased, the total diode capacitance is affected not only by the depletion capacitance, but also the bulk resistance which is frequency-dependent and associated with electron emission from slowly responding deep impurity levels. Furthermore at high frequencies the interface states cannot contribute to capacitance because the

IJSER

charge at the interface states cannot follow the a.c signal, therefore the capacitance at high frequencies is low as compared to low frequencies.

5.3.2 Voltage verses Conductance

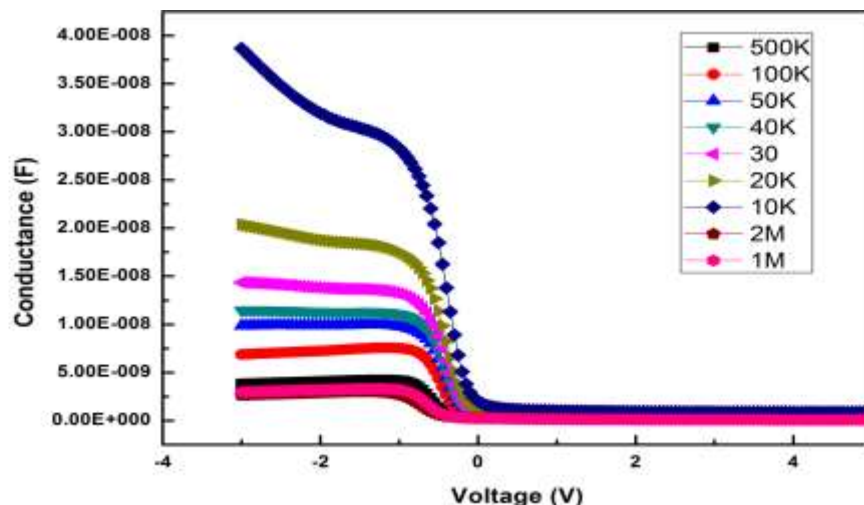

Figure 37 Conductance-Voltage (G-V) characteristics of Au/ZnO/Si Schottky diode at different frequencies

Fig. 37 shows the G-V characteristics of Ni/ZnO/Si Schottky contact at different frequencies and room temperature. The conductance of device is decreased as frequency increased. This behavior of conductance is attributed to particular distribution of interface states. From this plot it is also evident that positive voltage the conductance remained almost for all frequencies. Therefore it is concluded that at negative voltages the interface states are responsible of this conductance dispersion.

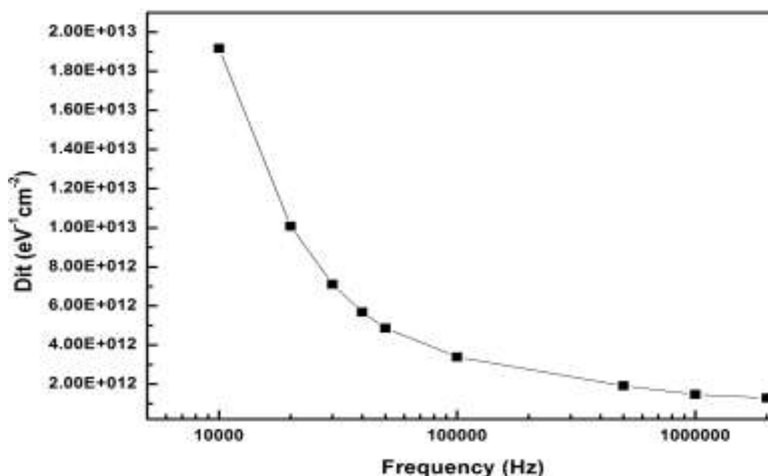

Figure 38 Frequency verses Dit plot of /ZnO/Si Schottky diode

The density of interface states can be determined by Hill-Coleman method. According to this method Dit can be calculated by the following formula [23]

$$Dit = 2Gc_{max/w}/qA[(Gc_{max/w}C_{ox})^2 + (1- C_c/C_{ox})^2]$$

Where A is the diode area, q is electronic charge, w is angular frequency, C_{ox} is the capacitance of oxide layer in accumulation region of C-V curves, $G_{c,\ max}$ maximum conductance of G-V curve and C_c is the capacitance of diode corresponding to $G_{c,\ max}$

Fig. 38 shows the density of interface states verses frequency. The calculated value of The Dit values decrease with increasing frequency. Similar results have been published in references

5.4 Deep Level Defects

In order to further investigate the nature and properties of deep level defects, we have chosen a sample with higher oxygen contents ratio (At% 54) verified by EDX. The temperature dependent Hall measurements were performed which showed the mix conductivity of sample. The SIMS measurements confirmed the presence of nitrogen traces in the sample. Nitrogen is considered the best p-type dopant in ZnO but the mechanism for p-type conductivity associated with N is

IJSER

very puzzling and still under debate because different activation sites of N have been reported in the band gap of ZnO. The most familiar sites are: nitrogen on oxygen site (N_O), nitrogen on Zn site (N_{Zn}), $N_O - V_{Zn}$, V_{Zn}-N_O-H^+ and cluster of four nitrogen atoms around Zn. Of these defect levels the chances of N_O and N_{Zn} to act as hole conductivity sources are minimal due to their exceptionally deep energy states (1.31 and 1.71 eV, respectively) [24, 25] in the band gap of ZnO. However, Park et al. [26] and Li et al.[27], using local density approximation (LDA) method reported N_O at lower energy levels at 0.40 eV and 0.31 eV, respectively. On the other hand, the N_O-V_{Zn} complex with energy level 0.40 eV above valence band maximum has been attributed (theoretically) to the double donor metastable state of N_{Zn}- V_O [28]. Similar explanation has been given by Reynolds et al. [29] for the H- induced transformation of N-V_{Zn} donor complex into V_{Zn}-N_O-H^+ as acceptor level at 0.13 eV. But, Reshchikov et al. [30] found experimentally an acceptor state in MBE grown N:ZnO at 0.40 eV but was attributed to V_{Zn} – complex. Recently, Muret et al. [31] reported a hole trap (HT5) with activation 0.48 eV and capture cross section 4.7×10^{-14} cm^2 using DLTS. They demonstrated that the defect was due to the involvement of nitrogen but real origin was not explained in their work. An overview of the current acceptor defect levels in ZnO and their possible origin can be found in Table I. It can be seen that the various nitrogen centers are scattered within band gap of ZnO and their origin is far from clear. Therefore the characterization of acceptor level states in ZnO is still of interest and still needs further investigation.

In this part of chapter, we report a new hole (acceptor) trap having activation energy 0.49±0.03 eV above the valence band for MBE-grown ZnO on Si determined by DLTS. Results Raman Scattering, photoluminescence and Secondary Ion Mass Spectroscopy (SIMS) of the ZnO layer

IJSER

indicate that the observed acceptor trap level is tentatively attributed to the nitrogen–zinc vacancy complex in ZnO.

DLTS is the most powerful and standard electrical techniques that provides quantitative information about the deep energy level position, capture cross-section and trap concentration.[21] Fig. 39 displays a typical DLTS spectra of an as-grown MBE ZnO layer measured under following conditions; U_R (reverse bias) = -1 V, Vp (filling pulse) = 0 V and t_p (filling time) = 20 seconds; lock-in frequency = 1500 Hz (3255s^{-1}) and biasing conditions were deliberately chosen as a way to avoid any contribution from Si substrate.

Table 10 Reported activation energy levels and origin of acceptor levels in nitrogen doped ZnO.

E_v+E_t (eV)	σ (cm^2)	Growth Technique	Characterization Method	Origin	References
0.48	4.7×10^{-14}	MBE	Experimentally: DLTS	N-related defect	31
0.19	3.0×10^{-15}	MBE	Experimentally: DLTS	N-related defect	31
0.40	-	MBE	PL	V_{Zn} related complex	30
1.70	-	SCV	PL	N_O	25
0.13	-	OMVPE	PL	V_{Zn}-N_O-H^+	29
1.30	-	-	DFT	N_O	24
0.40	-	-	DFT-LDA	N_O-V_{Zn}	28
0.40	-	-	DFT-LDA	N_O	26
0.31	-	-	DFT-LDA	N_O	27

0.49	8.6×10^{-18}	MBE	Experimentally: DLTS, PL, Raman, SIMS	N-V_{Zn}	This Study

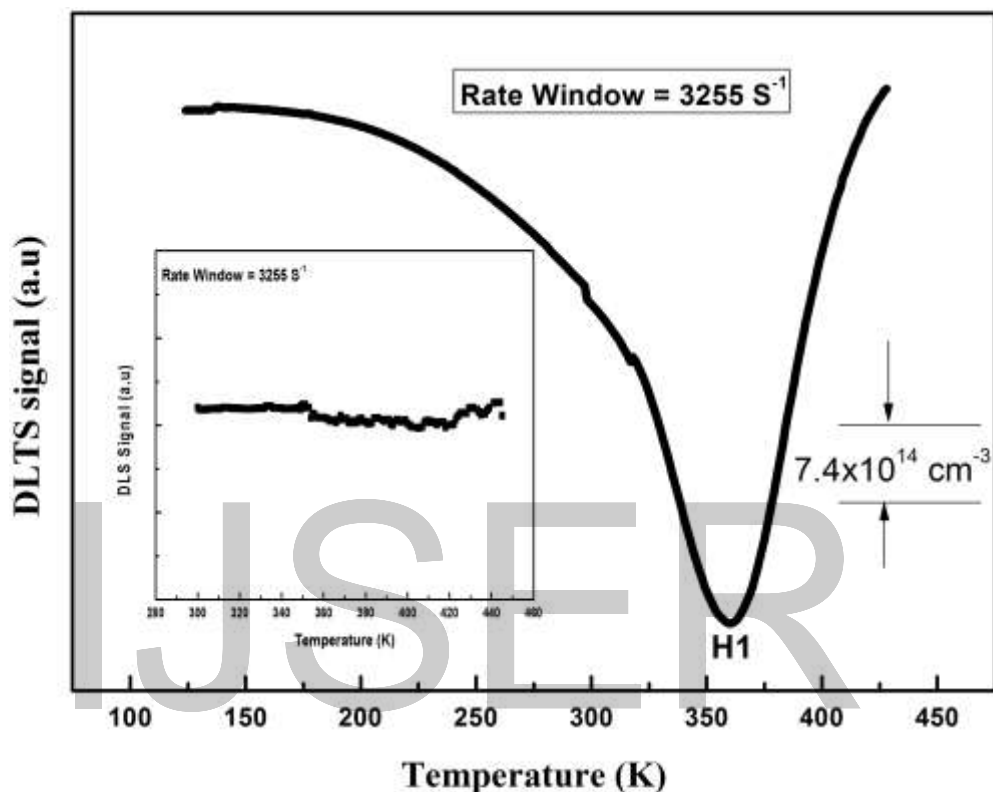

Figure 39 Typical DLTS spectra of ZnO thin film grown on Si substrate at 1500 Hz frequency (rate window 3255s-1). Inset shows the DLTS spectrum of Si at 1500 Hz in the same measuring conditions (Lock-in Principle)

One acceptor (hole) trap is observed at temperature 357K and referred as H1. The activation energy and trap capture cross section (trap concentration) determined from Arrhenius plot shown in Fig. 40 with values E_V+0.49±0.03 eV and 8.57×10^{-18} cm^{-2}($1.3\times10^{15}cm^{-3}$), respectively. Inset of the Figure 39 represents DLTS measurement performed on the clean part of the same wafer of Si, the DLTS spectrum is clean and hence confirms that H1 level clearly from ZnO layer.

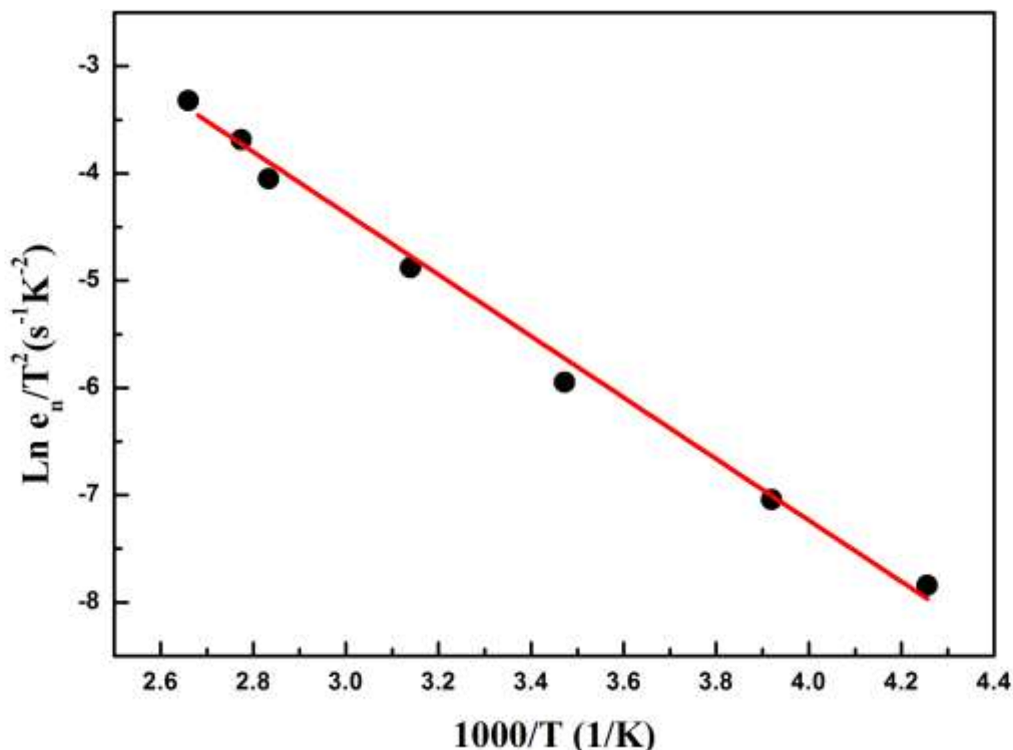

IJSER

Figure 40 Representative emission rate signatures (Arrhenius plot) of deep acceptor level H1 in MBE grown ZnO on Si substrate

The emission rate signatures together with the capture cross section of the defect and the SIMS results, suggest this defect is associated with nitrogen – Zn vacancy complex. It has been reported that in O-rich ZnO Zn-vacancies might have lower formation energy, therefore high density of Zn-vacancies in our O-rich ZnO is understandable [32]. It is also demonstrated in literature that N can form different energy levels in the whole band gap of ZnO [31]. We argue that at least one of nitrogen defect levels in ZnO exhibits metastable behavior and cannot be stable (manuscript under progress). This metastable N atom may form a complex with Zn-vacancy and appears at 0.49 eV above the valence band maximum. A hole defect with activation 0.48 eV and capture cross section 4.7×10^{-14} cm^2 using DLTS has been recently reported by Muret et al [31] and they called it N-related defects. Compared to Muret et al. [31] data, the much lower capture cross section (8.57×10^{-18} cm^{-2}) exhibited by H1 level in our sample gives

strong justification that Zn-vacancy and/or di-Vacancy might be involved with N ion. We also performed some additional measurements to support.

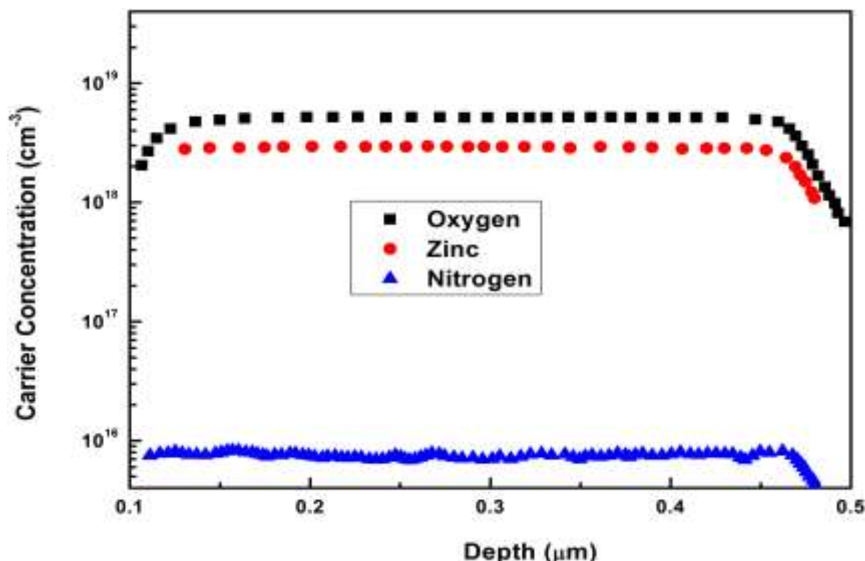

Figure 41 SIMS data of ZnO thin film grown on Si substrate by MBE demonstrates O, Zn and N ions with concentration (cm-3) ~ 1018, 1017 and 1016, respectively

IJSER

Fig. 41 shows the depth profile of oxygen, zinc and nitrogen revealed from SIMS measurement. Nitrogen atoms have diffused into throughout the 0.5 micron ZnO layer (the thickness of as grown ZnO layer), and have almost constant concentration throughout the film. Its concentration is appreciably reduced at the interface of ZnO film and Si substrate. Concentration of Zn, O and N species calculated from SIMS data was found to be ~ 10^{18} cm^{-3}, 10^{19} cm^{-3} and 10^{16} cm^{-3}, respectively and hence the presence of Zn vacancy in the layer is plausible. The reduction in the Zn content in the ZnO layer is probably due to nitrogen interplay during the growth. Whilst, the reason of introduction of nitrogen in MBE reactor is not clear, however, the involvement of nitrogen either in oxygen gas flow allowed into MBE chamber and/or relatively high base pressure (~10^{-6} Torr) cannot be avoided.

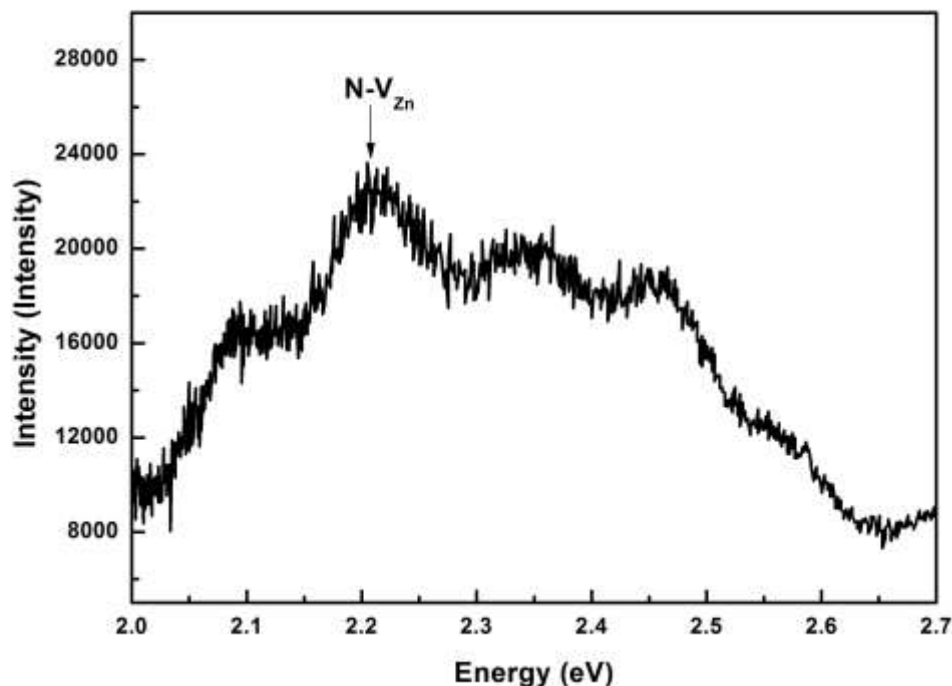

Figure 42Room temperature PL spectrum of MBE grown ZnO, peak at 2.2 eV is related to the N-Zn vacnacy complex

IJSER

Fig. 42 shows the room temperature PL spectrum of ZnO grown by MBE. The spectrum consists of two peaks at 2.2 and 3.28 eV (not shown here). We relate these peaks with defect emission and near band gap emission, respectively. We argue that defect emission peak at 2.2 eV is related to V_{Zn}-N defect complex. M. A. Reshchikov et al [30] demonstrated the origin of this peak in N-doped ZnO layers grown by MBE as the defect complex that may include a Zn-vacancy having activation energy 0.4 eV above the valence band. This activation energy of the reported defect complex was in fact, indirectly extracted by thermal shift of 2.2 eV YL band in PL measurement as function of temperature of the sample, we believe that this technique could not be as accurate as DLTS, therefore attribution of H1 with N-Zn-vacancy is more likely.

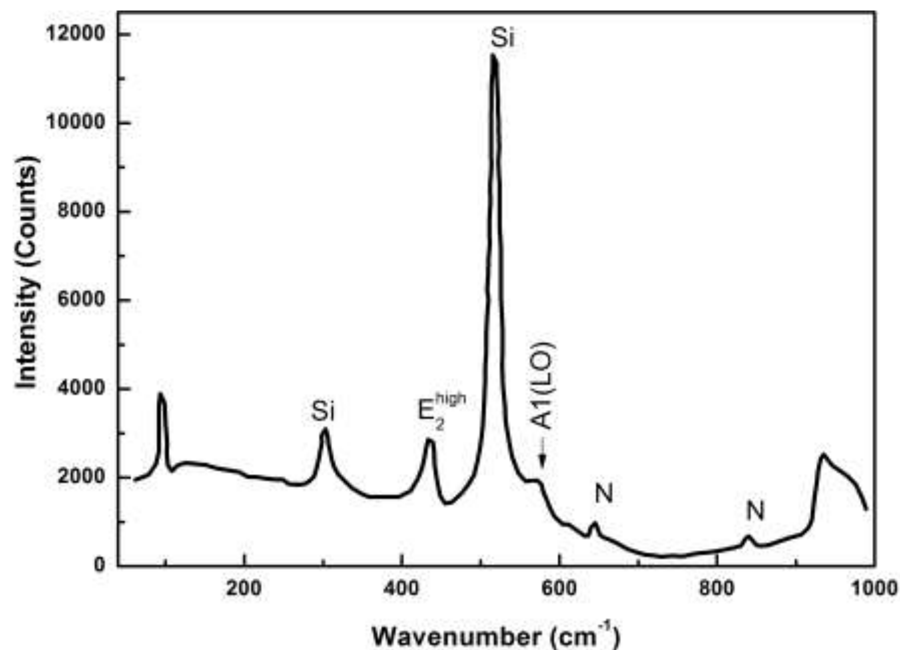

Figure 43 Raman scattering of MBE grown ZnO on Si substrate. The higher intensity of E_2^{high} mode as compared to A1(LO) mode demonstrated the O-rich status of sample

Raman spectroscopy of the layer is displayed in Fig. 43 which confirms the O-rich status of the ZnO due to higher intensity of E_2^{high} than that of A_1(LO) modes appearing at 437cm^{-1} and 577cm^{-1}, respectively [33]. Based on previous reports, peaks observed 643 cm^{-1} and 850 cm^{-1} in Figure 7 are attributed to nitrogen related defects [34-36]. Ke Yue Wu et al [35] and Friedrich et al [36] suggested that the vibrational mode at 275 cm^{-1} originates from Zn interstitials where parts of its nearest neighbor O atoms are replaced by N atoms to form Zn_i-N_O. Obviously this peak is absent in our samples being O-rich ones evidenced by SIMS and EDAX results in Figure 4. In this way, the presence of higher wavenumber Raman peaks (643 cm^{-1} and 850 cm^{-1} in Figure 6) strongly supports the connection of N-Zn vacancy type defects in ZnO. Rest of the peaks at 300 cm^{-1} and 512 cm^{-1} are related with silicon substrate [37, 38]. Relying on Raman data, we understand that our sample has Zn-vacancies and nitrogen related structural defect, henceforth, our argument related with the origin of H1 level to N-V_{Zn} complex is more likely.

5.5 Metastability Effect

We have also investigated time dependent behavior of this defect. It is observed that N-V_{Zn} deep level complex showed time dependent behavior, when measured after some time delayed

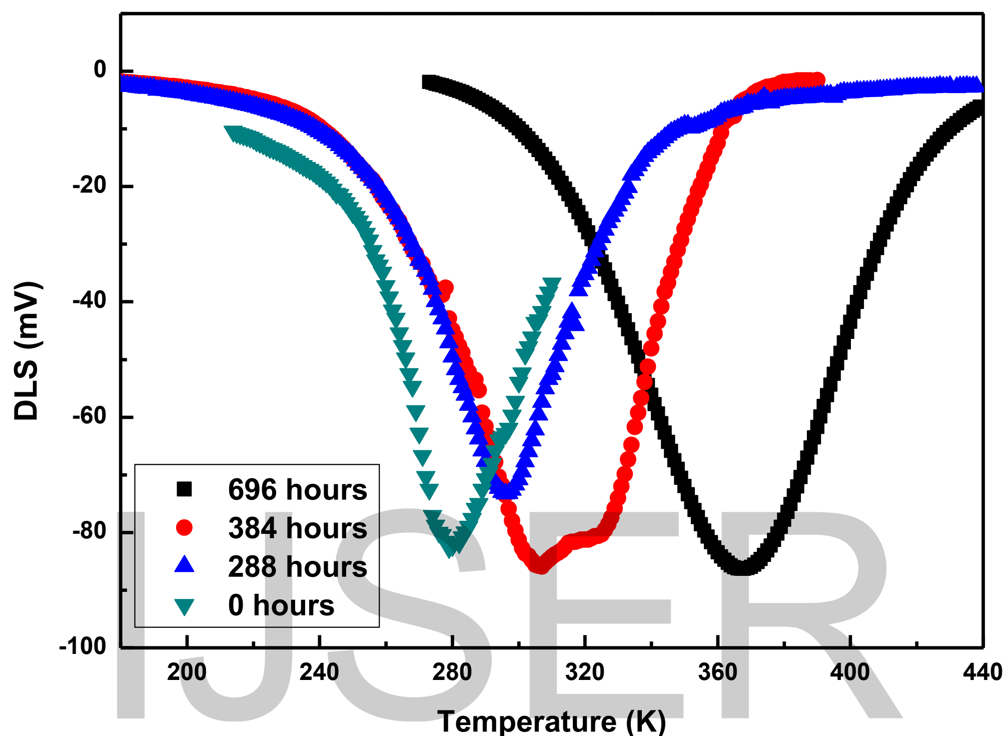

Figure 44 DLTS spectrum of MBE grown ZnO taken after different time

intervals. Fig. 44 shows the time dependent DLTS spectrum of MBE grown sample taken after 0, 288, 384 and 696 hours but rest of the conditions are similar. The graph evident that peak shifted towards high temperature. The Arrhenius plots of at different times have been drawn and shows in fig below

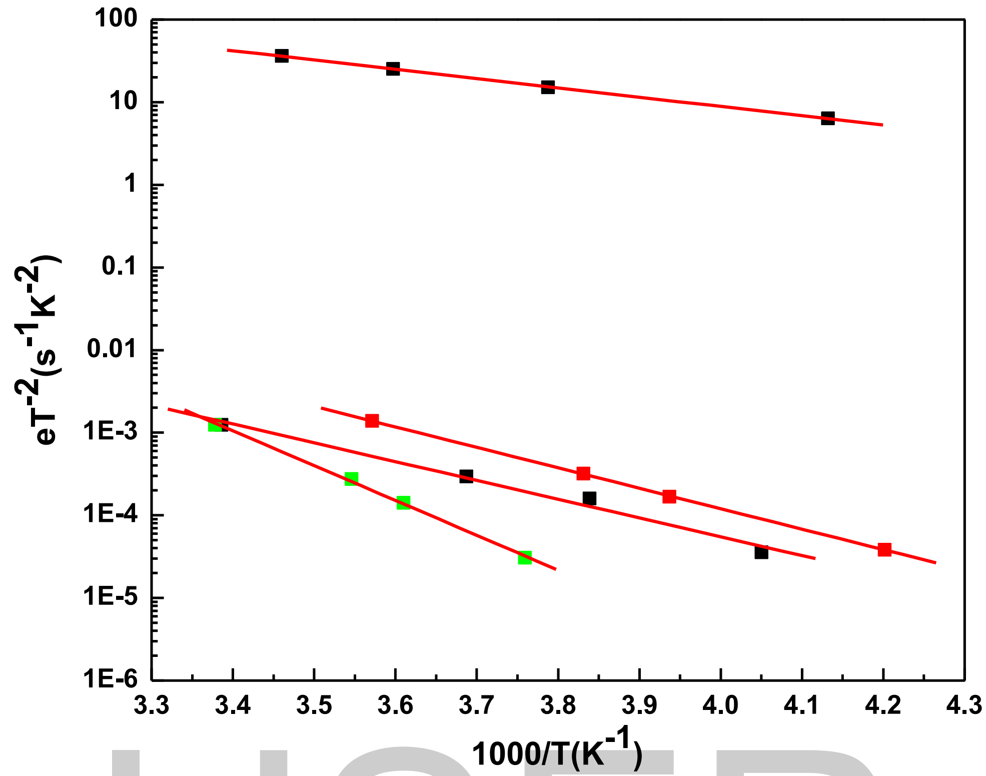

Figure 45Representative Arrhenius plots of deep acceptor level after time delayed

The activation energy of deep acceptor level was determined from the slope of Arrhenius plot shown in fig. 45. The value of activation energy was found to be 0.28, 0.32, 0.40 and 0.49 eV above the valence band after time 0, 288, 384 and 696 hours.

IJSER

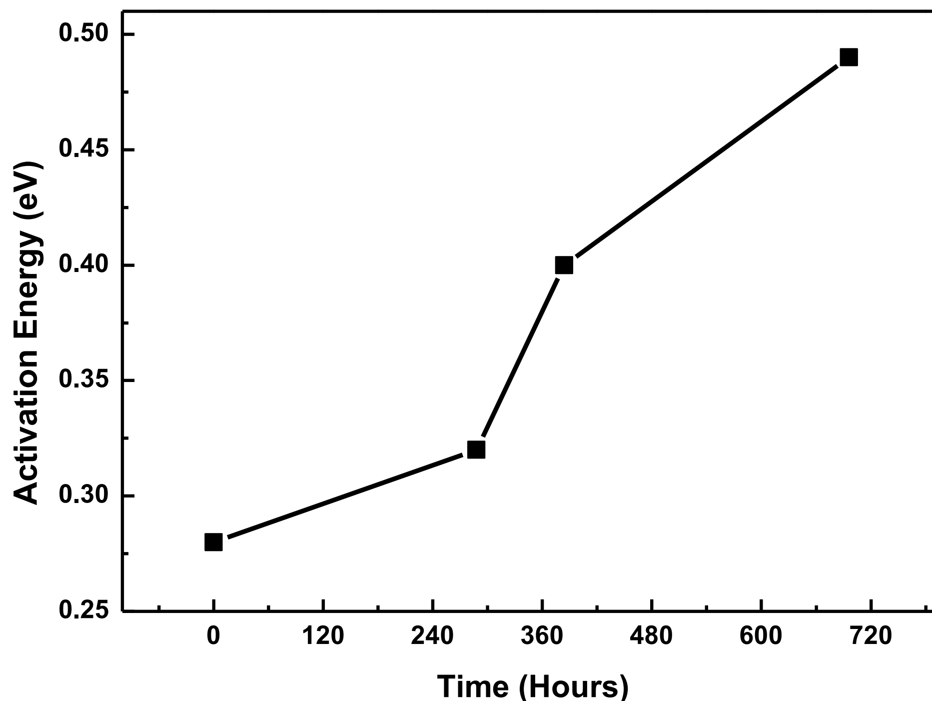

Figure 46Plot of time verses activation energy of deep acceptor level

The graph demonstrated that deep acceptor level changes its position with the passage of time. At first time measurement, the activation energy of level was found to be 0.28 eV above the valence band. But after few days it becomes deeper with activation energy 0.49 eV and which is stable state of this level. This metastable behavior of nitrogen related acceptor level is still under investigation.

IJSER

5.6 References

[1] A. Durmus, K. Ali, F.O. Ahmet, Microelectronic Eng. *B*. 98 (2012) 6-11

[2] Y.L. Jiang, Lu F. Ru, , X.P. Qu, B. Z. Li, W. Li, A.Z. Li, Chin. Phys. Lett. 19 (2002) 553–556.

[3] S. Chand, Kumar, J. Appl. Phys. 82 (1997) 5005–5010

[4] R.T. Tung, A.F.J. Levi, J.P. Sullivan, Schrey, Phys. Rev. Lett. 66 (1991) 72–75

[5] W. Mtangi, F.D. Auret, C. Nyamhere, P.J. Janse van Rensburg, A. Chawanda, M. Diale, J.M. Nel, W.E. Meyer, Physica B 404 (2009) 4402–4405

[6] H. Kima, H. Kim, D-W Kim, Vacuum 101 (2014) 92-97

[10] M. Asghar, K. Mahmood, F. Malik, M-A Hasan, J. Phys: Conf. Ser.439 (2013) 012030

[11] I. Tasçıoglu, S. Altındal, I. Polat, E. Bacaksız, Current Applied Physics 13 (2013) 1306-1310

[12] Z. Çaldıran, A.R. Deniz, S. Aydogana, A. Yesildag, D. Ekinc, Superlattices and Microstructures 56 (2013) 45–54

[13] S.J. Young, S.J. Chang, L.W. Ji, T.H. Meen, C.H. Hsiao, K.W. Liu, K.J. Chen, Z.S. Hu, Microelectronic Engineering 88 (2011) 113–116

[14] C. Tsiarapas, D. Girginoudi, N. Georgoulas, Materials Science in Semiconductor Processing 17 (2014) 199–206

[15] H. Tecimer, A. Türüt, H. Uslu, S. Altındal, I. Uslu, Sensors and Actuators A 199 (2013) 194–201

IJSER

[16] L. Shenn, H.W. Du, H. Ding, J. Tang, Z.Q. Ma, Materials Science in Semiconductor Processing 13 (2010) 339–343

[17] A. Kumar, S. Vinayak, R. Singh, Current Applied Physics 13 (2013) 1137-1142

[18] C. Coskun, N. Gedik, E. Balc, Semicond. Sci. Technol. 21 (2006) 1656–1660

[19] B. Roul, T.N. Bhat, M. Kumara, M.K. Rajpalke, N. Sinha, A.T. Kalghatgi, S.B. Krupanidhi, Solid State Communications 151 (2011) 1420–1423

[20] S. Aydogan, K. Cinar, H. Asıl, C. Coskun, A. Türüt, J. Alloy. Comp. 476 (2009) 913

[21] A. Bobby, S. Verma, K. Asokan, P.M.. Sarun, B.K. Antony, Physica B 431 (2013) 6–10

[22] F. Yakuphanoglu, Microelectronics Reliability 51 (2011) 2195–2199

[23] W.A. Hill A. C.C. Coleman, Solid-State Electron. 23 (1980) 987

[24] J. L. Lyons, A. Janotti and C. G. Van de Walle, Appl. Phys. Lett. 95 (2009) 252105

[25] M. C. Tarun, M. Zafar Iqbal, M. D. McCluskey, AIP Advances 1 (2011) 022105

[26] C. H. Park, S. B. Zhang, S. H. Wei, Phys. Rev. B 66 (2002) 073202

[27] J.B. Li, S.H. Wei, S-S. Li, and J.-B. Xia, Phys. Rev. B 74 (2006) 08120

[28] Lei Liu, Jilian Xu, Dandan Wang, Mingming Jiang, Shuangpeng Wang, Binghui Li, Zhenzhong Zhang, Dongxu Zhao, Chong-Xin Shan, Bin Yao and D. Z. Shen, Phys. Rev. Lett. 108 (2012) 215501

[29] J.G. Reynolds, C.L. Reynolds, Jr. A. Mohanta, J.F. Muth, J.E. Rowe, H.O. Everitt, D.E. Aspnes, Appl. Phys. Lett. 102 (2013) 152114

[30] M. A. Reshchikov, J. Q. Xie, B. Hertog, and A. Osinsky, J. Appl. Phys. 103 (2008)103514

IJSER

[31] P. Muret, D. Tainoff, C. Morhain, J-M. Chauveau, Appl. Phys. Lett. 101 (2012) 122104

[32] F. Oba, M. Choi, A. Togo, I. Tanaka, Sci. Technol. Adv. Mater. 12 (2011) 034302

[33] S. Dhara, P.K. Giri, Thin Solid Films, 520 (2012) 5000-5006

[34] J. Kennedy, D.A. Carder, A. Markwitz, R.J. Reeves, J. Appl. Phys. 107 (2010) 103518

[35] K.Y. Wu, Q.Q. Fang, W.N. Wang, C. Zhou, W.J. Huang, J.G. Li, Q.R. Lv, Y.M. Liu, Q.P. Zhang, H.M. Zhang, J. Appl. Phys. 108 (2010) 063530

[36] F. Friedrich. M.A. Gluba, N.H. Nickel, Appl. Phys. Lett. 95 (2009) 141903

[37] C. Wang, Z. Chen, H. Hua, D. Zhang, Physica B. 404 (2009) 4075

[38] M. Asghar, K. Mahmood, A. Ali, M-A Hasan, M. Y. A Raja, I. Hussain, M. Willander, ECS Trans. 35 (2011) 149-154

IJSER

Chapter 6 Concluding Remarks and Future Plans

US Department of Energy report said that we can save up 50 million US$ per year only in USA if all the current light sources are replaced by ZnO based lightening system. ZnO is still at bottleneck and waiting to enter in commercial market due to different issues associated with this material. The core issues are; origin of intrinsic n-type of conductivity, origin of visible emission and control of p-type conductivity. All these issues reported to be having routes in the intrinsic defects like oxygen vacancies, zinc interstitials, oxygen interstitials and V_O-Zn_i complex. Therefore the control and nature of intrinsic defects to rectify above said problems, is a major topic of research among the researchers.

7.1 Achieved Goals

In this dissertation, the effect of intrinsic defects on structural, optical, electrical and thermoelectric properties have been investigated in order to figure out the solution of ZnO material issues. A batch of samples with different Zn/O ratios was grown by molecular beam epitaxy. A representative wafer was cut into small pieces and subjected to different annealing conditions.

The major outcomes of this dissertation are;

- With increasing substrate temperature up to 500 ^{0}C, the quality of ZnO material improved significantly
- The structural properties degraded appreciably when samples grown with higher Zn/O ratio and after annealed in vacuum, zinc and vacuum+zinc environments but crystal quality improved while annealing in oxygen environment at different temperatures.
- Optical properties

IJSER

- Hall measurements suggested that carrier concentration increased with higher Zn/O ratio, annealing in vacuum, zinc and successively annealed in vacuum and zinc but decreased while annealed in oxygen environment at different temperature. A defect donor complex V_O-Zn_i was identified as source of intrinsic n-type conductivity of ZnO.

- The detailed Schottky contacts properties of Au/ZnO/Si diodes have been investigated and found that Schottky diodes deviated from ideal behaviors which were fabricated on samples having higher Zn/O contents ratio. But all samples same nature of deep level defects with activation energy 0.58 eV below the conduction band.

- A deep acceptor level with activation energy 0.49 eV above the valence band was observed is a sample with higher oxygen At%. The defect was identified as N-V_{Zn} complex.

- The value of Seebeck coefficient, power factor and figure of merit enhanced with annealing temperature up to 800 ^{0}C and decreased while annealed in vacuum and zinc environments.

In general conclusion, the origin of defect emission, intrinsic n-type and cause of p-type of conductivity have been successfully investigated. Furthermore the effect of intrinsic defects on structural, optical, electrical and thermoelectric properties demonstrated in detail. It is believed, on the basis of results presented in this dissertation, that hurdles on the road to commercialization of ZnO have been minimized.

IJSER